Grain-Size and -Shape, Median Diameter, and Proportion of Pumice and Lithic Fragments as a Key to Movement and Emplacement Mechanism of Pumice Flow Deposits : The "Shirasu" Pumice Flow Deposits in Kyushu, Japan

Taneda, Sadakatu
Faculty of Science, Kyushu University

Grain-Size and -Shape, Median Diameter, and Proportion of Pumice and Lithic Fragments as a Key to Movement and Emplacement Mechanism of Pumice Flow Deposits

—The "Shirasu" Pumice Flow Deposits in Kyushu, Japan—

Sadakatu TANEDA

Abstract

In my previous papers, I inferred that the "Shirasu" proper is a deposit formed by a succession of abnormal explosions, perhaps of the nueé ardente or pumice flow type, from the "Aira caldera" (S. TANEDA, 1954, 1957, 1971, etc.). I pointed out that the distinction between normal and abnormal type of volcanic activity is reflected usually in the field relationships and mechanical analyses of the erupted matters.

In the course of research of the "Shirasu", I measured a, b, c, l and s for ten largest pumice fragments and ten largest lithic fragments per square meter (1 m×1 m) at each outcrop. Here a, b and c are long diameter (length), intermediate diameter (breadth), and short diameter (thickness) (ZINGG, 1935), respectively. The arithmetic means of each set of ten measurements were calculated, which are called the average of a, b, c, l and s respectively, and marked by a_P^{av}, b_P^{av}, c_P^{av}, l_{P1}, l_P^{av}, s_P^{av}, for pumice fragments and by a_L^{av}, b_L^{av}, c_L^{av}, l_{L1}, l_L^{av}, s_L^{av} for lithic fragments. The l_{P1}, l_P^{av} and l_{L1}, l_L^{av} values are called the apparent maximum size of pumice and lithic fragments. The proportion of pumice and lithic fragments of the "Shirasu" pumice flow deposists (NPF, NLF, NPC and NLC), and median diameter (Md) are also inspected.

The areal variation patterns are obtained by the following methods.

The southern part of Kyushu was divided into nearly 600 squares by drawing on the map north-south and east-west lines at every 5 km. In each square covered by the pumice flow deposits "Shirasu", one or more (up to several) outcrops of the deposits were selected for the grain-size, median diameter and shape measurements, and for the proportion of pumice and lithic fragments of the "Shirasu".

The data obtained are plotted on the map at the outcrop location, and the arithmetic mean of data is calculated for every square.

In order to reduce the effect of local irregularities of the data variation, the overlapping means are used.

As to the kinds of areal variation patterns, are constructed such six kinds of diagrams as a "Data map", b "Hatching diagram", c "Hatching diagram" using the overlapping means, d "Contour lines", e "Contour lines" using the overlapping means, and f "Ridge and valley lines" using the overlapping means.

In this report the areal variations with respect to the distance from their source for maximum grain-size and shape, median diameter and proportion of pumice and lithic fragments of the "Shirasu" pumice flow deposits (l_{P1}, l_P^{av}, l_{L1}, l_L^{av}, l_P^{av}/s_P^{av}, l_L^{av}/s_L^{av}, l_P^{av}/l_L^{av}, Md, NPF. NLF, NPC. NLC) are discussed. Plots of these data seem to give qualitative information on the variables involved in the ejection, transportation and deposition of pyroclastic fragments. The areal variation patterns show the concentric and radial characters suggesting the source locality (the Aira caldera). One of the most significant conclusion is

that the increasing of grain-sizes of the "Shirasu" along with the increasing distance is caused by the emission effect of gas included in ejecta, because by the mechanism of the gas-emission hypothesis large blocks should travel farther than small ones. Comparing with the pumice fragments, the lithic fragments begin to settle rather early from the flow according to their grain-size, because of their larger density than that of the matrix.

Contents

I. Introduction

In my previous papers (TANEDA, 1954, 1957, 1971, 1975; TANEDA, et al., 1957, 1970, etc.), I gave the geological and petrological outlines of the "Shirasu", the wide-spread loose tuffaceous deposits forming a vast table land in south Kyushu, and inferred that the "Shirasu" proper is a deposit formed by a succession of abnormal explosions, perhaps of the nueé ardente or pumice flow type, from the "Aira caldera".

The distinction between normal and abnormal types of volcanic activity does or does not reflect in the chemical and mineral composition but it is reflected usually in the field relationships and mechanical analyses of the erupted matters. (FISHER, 1964; VERHOOGEN, 1951; MOORE, 1934; TANEDA, 1954, 1957, 1971, 1975, etc.)

In this report the areal variations—with respect to the distance from their source—of maximum grain-size and -shape, median diameter and proportion of pumice and lithic fragments of the "Shirasu" pumice flow deposits are discussed. Plots of these data seem to give qualitative information on the variables involved in the ejection, transportation and deposition of pyroclastic fragments, which is valuable for the research of the movement and emplacement mechanism of the so-called abnormal volcanic eruption products.

This paper is a part of my contribution to the research of the "Shirasu" carried out since 1950. The study mainly on the grain-size and -shape of the "Shirasu" has begun in 1957, and most field measurements were carried out mainly before 1970, and then the laboratory works during several years. They were supported by the Grant in Aid for Scientific Researches from the Ministry of Education, Japan. A part of data were obtained by assistance of Late Dr. MIYACHI, Mrs. MIYACHI and Mr. MORITA during my field works in 1958, to whome I am indebted. Miss Y. IWABUCHI and Mrs. E. ABE helped me for the figures drawing.

II.   Methods of Measurement of Grain-size and -shape, Median Diameter and "Proportion" of Pumice and Lithic Fragments ; and Construction of Areal Variation Patterns

1.   Roughly speaking, the "Shirasu" has a general appearance of either loose lapilli tuff, or loose tuff breccia, or loose volcanic breccia, with a conspiquous

Table 2.1.   Nomitation of l, s, a, b and c for ten largest fragments in measured 1m section.

		1	2	3	4	5	6	7	8	9	10	av
Pumice fragments	apparent (in a section) long diameter (l)	l_{P1}	l_{P2}	l_{P3}	l_{P4}	l_{P5}	l_{P6}	l_{P7}	l_{P8}	l_{P9}	l_{P10}	l_P^{av}
	short diameter (s)	s_{P1}	s_{P2}	s_{P3}	s_{P4}	s_{P5}	s_{P6}	s_{P7}	s_{P8}	s_{P9}	s_{P10}	s_P^{av}
	true long diameter (a)	a_{P1}	a_{P2}	a_{P3}	a_{P4}	a_{P5}	a_{P6}	a_{P7}	a_{P8}	a_{P9}	a_{P10}	a_P^{av}
	intermediate (b)	b_{P1}	b_{P2}	b_{P3}	b_{P4}	b_{P5}	b_{P6}	b_{P7}	b_{P8}	b_{P9}	b_{P10}	b_P^{av}
	short diameter (c)	c_{P1}	c_{P2}	c_{P3}	c_{P4}	c_{P5}	c_{P6}	c_{P7}	c_{P8}	c_{P9}	c_{P10}	c_P^{av}
Lithic fragments	apparent (in a section) long diameter (l)	l_{L1}	l_{L2}	l_{L3}	l_{L4}	l_{L5}	l_{L6}	l_{L7}	l_{L8}	l_{L9}	l_{L10}	l_L^{av}
	short diameter (s)	s_{L1}	s_{L2}	s_{L3}	s_{L4}	s_{L5}	s_{L6}	s_{L7}	s_{L8}	s_{L9}	s_{L10}	s_L^{av}
	true long diameter (a)	a_{L1}	a_{L2}	a_{L3}	a_{L4}	a_{L5}	a_{L6}	a_{L7}	a_{L8}	a_{L9}	a_{L10}	a_L^{av}
	intermediate (b)	b_{L1}	b_{L2}	b_{L3}	b_{L4}	b_{L5}	b_{L6}	b_{L7}	b_{L8}	b_{L9}	b_{L10}	b_L^{av}
	short diameter (c)	c_{L1}	c_{L2}	c_{L3}	c_{L4}	c_{L5}	c_{L6}	c_{L7}	c_{L8}	c_{L9}	c_{L10}	c_L^{av}

l^{av} : l_P^{av} or l_L^{av} $\qquad$ s^{av} : s_P^{av} or s_L^{av}

a^{av} : a_P^{av} or a_L^{av} $\qquad$ b^{av} : b_P^{av} or b_L^{av} $\qquad$ c^{av} : c_P^{av} or c_L^{av}

"Maximum grain-size" for pumice fragments and lithic fragments.

$\quad$ l_{P1} : Apparent long diameter of the largest pumice fragment in a 1m² outcrop section.

$\quad$ l_P^{av} : Average of apparent long diameters of ten largest pumice fragments in a 1m² outcrop section.

$\quad$ l_{L1} : Apparent long diameter of the largest lithic fragment in a 1m² outcrop section.

$\quad$ l_L^{av} : Average of apparent long diameters of ten largest lithic fragments in a 1m² outcrop section.

"Size proportion" of pumice fragments to lithic fragments.

$\quad$ l_P^{av}/l_L^{av} : The ratio l_P^{av}/l_L^{av}.

"Grain-shape" (Degree of deviation from "equant" form) for pumice and lithic fragments.

$\quad$ l_P^{av}/S_P^{av} : The ratio l_P^{av}/S_P^{av} of pumice fragments.

$\quad$ l_L^{av}/S_L^{av} : The ratio l_L^{av}/S_L^{av} of lithic fragments.
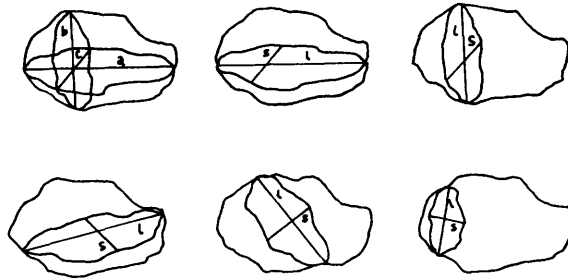
Fig. 2.1 a: long diameter for a fragment.
         b: intermediate diameter (do.)
         c: short diameter (do.)
         l: large diameter in a section (apparent long diameter).
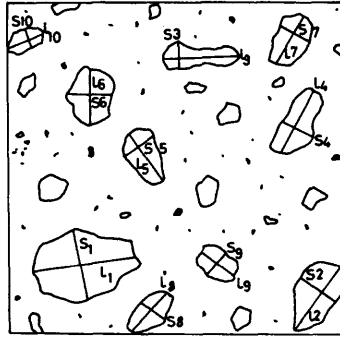   s: small diameter (do.) (apparent short diameter).

Fig. 2.2 Sketch showing the method of l and s measure-
          ment of ten largest fragments in 1m² section at
          each outcrop.

proportion of pumiceous and compact (lithic) fragments.

In the course of research of the "Shirasu" (a pumice flow deposit, non-welded) I measured a, b, c, l and s for ten largest pumice fragments and ten largest lithic fragments per square meter (1 m×1 m) at each outcrop. Here a, b and c are long diameter (length), intermediate diameter (breadth), and short diameter (thickness) (ZINGG, 1935), respectively, as shown in Figs. 2.1. and 2.2. The arithmetic means of each set of ten measurements were calculated, which are called the average of a, b, c, l and s respectively, and marked by a_P^{av}. b_P^{av}, c_P^{av}, l_P^{av}, s_P^{av} for pumice fragments and by a_L^{av}, b_L^{av}, c_L^{av}. l_L^{av}. s_L^{av} for lithic fragments (Tables 2.1 and 2.2). The l_{P1}, l_P^{av} and l_{L1}, l_L^{av} values are called the maximum size of pumice and lithic fragments, respectively.

The relations of l_{P1} to l_P^{av} and of l_{L1} to l_L^{av} are as follows (TANEDA, 1971):

$$l_P^{av} \fallingdotseq l_{P1} \times 0.6 \text{ for } l_P^{av} < 6 \text{ cm}, \ l_{P1} < 10 \text{ cm}.$$

$$l_P^{av} \fallingdotseq l_{P1} \times 0.175 + 5 \text{ cm for } l_P^{av} > 7.5 \text{ cm}, \ l_{P1} > 15 \text{ cm}.$$

$$l_L^{av} \fallingdotseq l_{L1} \times 0.5 \text{ for } l_L^{av} < 2 \text{ cm}, \ l_{L1} < 4 \text{ cm}.$$

$$l_L^{av} \fallingdotseq l_{L1} \times 0.15 + 1.5 \text{ cm for } l_L^{av} > 2.5 \text{ cm}, \ l_{L1} > 5 \text{ cm}.$$

There are some unique relations among the respective averages of a, b, c, l and s, as shown below (TANEDA, 1971).

$$a_P^{av} \fallingdotseq 1.2 \times l_P^{av}$$
$$a_L^{av} \fallingdotseq 1.2 \times l_L^{av}$$
$$c_P^{av} \fallingdotseq s_P^{av} \text{ (for } < 4.5 \text{ cm)} \sim 0.857\ s_P^{av} + 0.5 \text{ cm (for } s_P^{av} > 4.5 \text{ cm)}$$
$$c_L^{av} \fallingdotseq s_L^{av} \text{ (for } < 4.5 \text{ cm)} \sim 0.857\ s_L^{av} + 0.5 \text{ cm (for } s_L^{av} > 4.5 \text{ cm)}$$
$$l_P^{av}/s_P^{av} \fallingdotseq 0.68\ a_P^{av}/c_P^{av} + 0.32 \fallingdotseq 1.66\ (a_P^{av} + b_P^{av})/(b_P^{av} + c_P^{av}) - 0.66$$
$$l_L^{av}/s_L^{av} \fallingdotseq 0.68\ a_L^{av}/c_L^{av} + 0.32 \fallingdotseq 1.66\ (a_L^{av} + b_L^{av})/(b_L^{av} + c_L^{av}) - 0.66$$

Therefore it is to be noticed that the l^{av}/s^{av} ratios can be used as an indicator of deviation degree from the "equant form". Generally speaking l^{av} and s^{av} are valuable for research of the size and shape of fragments of pyroclastics as well as sediments.

The median diameters ("Md") are obtained by mechanical analysis of the matrix corresponding to the tuffaceous fraction (<4 mm), excluding the coarse fragments (>4 mm). The proportion of pumice and lithic fragments means the proportion of the number of pumice fragments to the number of lithic fragments per unit area at each outcrop (the ratios NPF/NLF and NPC/NLC).

NPF: The number of pumice fragments (32~4 mm) per square meter (1 m²) at each outcrop.

NLF: The number of lithic fragments (32~4 mm) per square meter (1 m²) at each outcrop.

NPC: The number of pumice coarse-ashes (4~2 mm) per square decimeter (10 cm×10 cm) at each outcrop.

NLC: The number of lithic coarse-ashes (4~2 mm) per square decimeter (10 cm×10 cm) at each outcrop.

2. The areal variation patterns are obtained by the following methods, for maximum grain-size and grain-shape, median diameter and proportion of pumice and lithic fragments.

The southern part of Kyushu was divided into nearly 600 squares by drawing on the map north-south and east-west lines at every 5 km. In each square covered by the pumice flow deposits "Shirasu", one or more (up to several) outcrops of the deposits were selected for the grain-size, median diameter and shape measurements. The locations of these outcrops are shown in Fig. 2.3.

The data obtained are plotted on the map at the outcrop location, and the arithmetic mean of data is calculated for every square.

In order to reduce the effect of local irregularities of the data variation, the overlapping means are used.

As to the kinds of areal variation patterns, are constructed such six kinds of diagrams as a "Data map", b "Hatching diagram", c "Hatching diagram" using the overlapping means, d "Contour lines", e "Contour lines" using the overlapping means and f "Ridge and valley lines" using the overlapping means.

III. "Maximum grain-size" (l_{P1}, l_P^{av}, l_{L1}, and l_L^{av}) and "Size proportion" of Pumice and Lithic Fragments (l_P^{av}/l_L^{av})

The areal variation of the "maximum grain-size for pumice and lithic fragments (l_{P1}, l_P^{av}, l_{L1}, and l_L^{av}), and the "size proportion" of pumice fragments to lithic ones (l_P^{av}/l_L^{av}) are shown in Figs. 3.1.a~f, 3.2.a~f, 3.3.a~f, 3.4.a~f and 3.5.a~f, respectively. It is to be noted that each of them shaws a well-or ill-defined concentric pattern and partial radial one around the so-called "Aira caldera" which is now represented by the northern part of Kagoshima Bay.

As regards the relation of grain-size and the distance from the source, the maximum variation range is seen at a certain distance and the grain-size tends to decrease therefrom (KUNO, et al. (with TANEDA), 1964); in this paper it is concluded that the maximum grain-size tende to increase along with the distance from the source (the central part of the Aira caldera) increases to reach the peak at a certain distance, and decrease therefrom toward the outer limit of the deposits. Here the distance of the peak from the source is about 20~40 km for pumice fragments (l_{P1}, l_P^{av}) and about 10~20 km for lithic fragments (l_{L1}, l_L^{av}).

The size proportion of pumice fragments to lithic fragments (l_P^{av}/l_L^{av}) tends to increase along with increase of the distance from the source (the tentative center of the Aira caldera).

l_{P1} Variation range: 34.0~2.7 cm, maximum 34 cm between 20 and 40 km from the source.

Average for main part: 5 cm (at 10 km*), 16 cm (peak at about 30 km*), 3 cm (at 70 km*).

l_P^{av} Variation range: 11.3~0.9 cm, maximum 11.3 cm between 20 and 40 km*.

Average for main part: 3.5 cm (at 10 km*), 7.5 cm (peak at about 30 km*), 1.5 cm (at 70 km*).

l_{L1} Variation range: 21.0~0.4 cm, maximum 21.0 cm between 10 and 20 km*.

Average: 5 cm (at 10 km*), 7.5 cm (peak at about 15 km*), 1 cm (at 70 km*).

l_L^{av} Variation range: 5.4~0.1 cm, maximum 5.4 cm between 10 and 20 km*.

Average: 2.5 cm (at 10 km*), 3.5 km (peak at about 15 km*), 0.3 cm (at 70 km*).

l_P^{av}/l_L^{av} Variation range: 15.5~0.7, increasing along with the distance. Max. 15.5 at 50 km*.

Average for main part: 1.5 (at 10 km*), 6.5 (at 50 km*), 7.5 (at 70 km*).

---

* km shows the distance from the source (the tentative center of the Aira caldera which is approximately 20 km in diameter).

IV. "Grain-shape" of Fragments (the ratios l_P^{av}/s_P^{av} and l_L^{av}/s_L^{av})

As above mentioned the ratio $l^{av} s^{av}$ can be used as indicator of deviation degree from the "equant form".

The areal variations of the ratios l_P^{av}/s_P^{av} and l_L^{av}/s_L^{av} of the pumice and lithic fragments of the "Shirasu", respectively, are shown in Figs. 4.1.a~f, 4.2.a~f. These diagrams show the ill-defined concentric patterns and a partial radial ones around the Aira caldera.

The mode of concentric patterns for l^{av}/s^{av} are rather complicated; the center of the pattern is deviated from the center of Aira caldera a little southwards and one of the local peaks is found at the northern rim of the caldera.

As regards the tendency of variation along with the increase of the distance from the source, the ratio l_P^{av}/s_P^{av} (for pumice fragments) tends to gently increase toward the outer limit of the deposits with exception of central part, in which besides the increasing trend is found a tendency of decreasing with the increase of the distance, but ratio l_L^{av}/s_L^{av} (for lithic fragments) decreases along with the distance increases.

l_P^{ra}/s_P^{av} Variation range: 3.3~1.3, gently increasing with the distance from the source.

upper limit, 2.9 (at 10 km*), 3.3 (at 45 km*); lower limit, 1.3 (at 25~45 km*), 1.4 (at 65 km*).

Average for main part: 1.7 (at 10~50 km*).

l_L^{av}/s_L^{av} Variation range: 2.1~1.0, decreasing with the distance from the source.

Average: 1.7 (peak ? at 12 km*), 1.2 (at 70 km*).

V. "Median Diameters (Md)"

The areal variation of Md for tuffaceus fraction less than 4 mm in size are shown in Figs. 5.1.a~f. Here the coarse fragments larger than 4 mm in diameter are excluded.

It is to be noted that the areal variation pattern for Md is concentric around the Aira caldera and that Md decreases along with the distance from the source increases.

Md   Variation range: 0.72~0.15 mm, decreasing with increase of the distance form the source.

Average for main part: 0.42 mm (peak ? at 12~18 km*), 0.23 (at 70 km*). (for tuffaceous fraction, <4 mm in diameter).

VI. "Proportions of Pumice and Lithic Fragments" (NPF/NLF and NPC/NLC)

The proportion of the number of pumice and lithic fragments per unit area at each outcrop were measured.

The ratio NPF/NLF is used for the numbers of fragments (32~4 mm in size) per square meter (1 m²) and the ratio NPC/NLC is used for the numbers of

coarse ashes (4~2 mm) per square decimeter (10 cm²).

The areal variation patterns are concentric and radial, surrounding the Aira caldera as shown in Figs. 6.1.a~f and 6.2.a~f.

It is notable that the ratio NPF/NLF tends to increase with increasing distance from the caldera toward the outer side, but the ratio NPC/NLC tends to increase along with the distance from the source increases to reach the peak at a certain distance (about 30 km), and decreases therefrom toward the outer limit of the deposits.

The decrease of the ratio NPC/NLC should be in accordance with the increase of the density of the matrix (<4 mm in size) against fragments (32~4 mm) of the deposits.

> NPF/NLF Variation range: (270~) 32~1, increasing with increase of the distance from the source.
> Average: 2.5 (at 10 km*), 20.0 (approximately at 70 km*).

> NPC/NLC Variation range: 6.5~ 0.1, decreasing with increase of the distance from the source.
> Average for main part: 2.5 (at 10~20 km*), 0.4 (at 70 km*).

VII. Mechanism of Movement and Emplacement of "Shirasu" Pumice Flow Deposits

1. The values of the l_{P1}, l_P^{av}, l_{L1}, l_L^{av}, l_P^{av}/l_L^{av}, l_P^{av}/s_P^{av}, l_L^{av}/s_L^{av}, Md, NPF/NLF and NPC/NLC are variable, ranging rather broadly as above mentioned and as shown in Table 7.1.a~b. It is to be noted that the areal variations tend to show the concentric and radial patterns around the Aira caldera which is now represented by

Table 7.1.a Variation range of the values.

	A	B
	Arithmetic means per each unit square (5km× 5km)	Overlapping means for A
l_{P1}	34.0~2.7 cm	21.3~3.4 cm
l_P^{av}	11.3~0.9 cm	10.4~1.2 cm
l_{L1}	21.0~0.4 cm	11.3~0.5 cm
l_L^{av}	5.4~0.1 cm	3.3~0.3 cm
l_P^{av}/l_L^{av}	15.5~0.7	11.3~1.3
l_P^{av}/s_P^{av}	3.3~1.3	3.3~1.3
l_L^{av}/s_L^{av}	2.1~1.0	2.0~1.1
Md*	0.72~0.15 mm	0.56~0.18 mm
NPF/NLF	(270~) 20.0~1.0	(138~) 15.0~1.4
NPC/NLC	6.5~0.1	6.5~0.1

* for tuffaceous fractions (<4 mm in size).

Table 7.1.b Distance from the caldera rim (Km)

Radial Division (Fig. 7-1)	Peak	
	l_P^{av}	l_L^{av}
I	10~20	5~15
II	15	8~13
III	20~30	
IV	20~27	
V	15~23	
VI	10~15	
VII	10~15	10
VIII	8	8
IX	20~30	
X	10~15	10
	8~30	5~15

the northern part of the Kagoshima Bay. It is important that the eruption source of the "Shirasu" pumice flow deposits is considered to be the Aira caldera which is about 10 km in radius.

2. The maximum grain-size of fragments (l_{P1}, l_P^{av}, l_{L1}, l_L^{av}) increase along with the distance from the source increases to reach the peak at a certain distance and decrease therefrom toward the outer limit of the deposits. The distance of the peak from the source is about 20~40 km for pumice fragments and 10~20 km lithic fragments.

K. C. McTAGGART (1960) pointed out that on the gas-emission hypothesis, there should be a regular distribution with respect to the volcano, in which the largest blocks are more distant from the source, but such a required sort of distribution has not been reported. I think that the increasing of grain sizes of the "Shirasu" just mentioned along with the increasing distance is caused by the emission effect of gas included in ejecta because by the mechanism of the gas-emission hypothesis large blocks should travel farther than small ones. The difference between the peak distance of pumice fragments from that of lithic ones is attributed to the difference of density (Pumice < Lithic fragment in density). In the period of grain-size increasing (the pre-peak period) the effect of gas-emission overwhelms the gravity-effect, although in the period of grain-size decreasing (the post-peak period) the latter (the gravity-effect) predominates.

3. As to the gravity effect, the fact that the NPF/NLF ratio is larger than the NPC/NLC ratio suggests that large pumice fragments are floatable or suspensible against the mixture of pumice and lithic particles, because the bulk density is larger than the coarse pumice fragments.

The lithic fragments begin to settle rather early from the flow according to their grain-size, because of their larger density than that of the matrix.

The difference between l_P^{av}/l_L^{av}, l_P^{av}/s_P^{av} and l_L^{av}/s_L^{av} in variation pattern (III and IV in pp. 114~115), are interpreted as due to the density difference between the two types of fragments carried in the pumice flow deposits, according to the gas

emission and gravity mechanism.

4. Here the topographic effect was inspected by overlapping the topographic map (Fig. 2.4) upon each diagram (Figs. 3.1~5, 4.1~2, 5.1, 6.1~2).

The relations among the grain-size, -shape, median diameter and the basement topography seem to be too complicated to analyse; generally speaking, it may be better to say that the general relation or regurality is hardly found; and no discussion is given here.

References cited

FISHER, R. V. (1964) :   Maximum Size, Median Diameter, and Sorting of Tephra. Jour. Geoph. Res., 69, 341–355.

KUNO, H., ISHIKAWA, T., KATSUI, Y., YAGI, K., YAMASAKI, M. & TANEDA, S. (1964) : Sorting of pumice and Lithic Fragments as a Key to Eruptive and Emplacement Mechanism. Jap. Jour. Geol. Geog., 34, 223–238.

McTAGGART, K. C. (1960) :   The Mobility of Nueés Ardentes. Amer. Jour. Sci., 258, 369–382.

———— (1962) :   Nueés Ardentes and Fluidization (Reply). Ibid., 260, 470–476.

MOORE, B. N. (1934) :   Deposits of possible, Nueé Ardente origin in the Crater Lake Region, Oregon. Jour. Geol., 42, 355–357.

TANEDA, S. (1954) :   Geological and petrological Studies on the "Shirasu" in South Kyushu, Japan. Part I. Mem. Fac. Sci., Kyushu Univ., Geol., 4, (2), 167–177.

———— (1957) :   Do., Part II. Ibid., 6, (2), 91–105.

TANEDA, S., MIYACHI, S. & NISHIHARA, M. (1957) :   Do., Part III. Ibid., 6, (2), 107–127.

TANEDA, S., MIYACHI, M., MORITA, J. & IRISA, S. (1970) :   Do., Parts IV–VII. Ibid., 20, (1), 145–157.

TANEDA, S. (1975) :   Do., Part VIII. Ibid., 23, (2), 295–301.

TANEDA, S. (1971) :   Studies on the size and shape of the fragments of the pyroclastic flow deposits ("Shirasu" and "Hai-ishi") (in Japanese). Sci. Repts. Shimabara Volc. Observ., Fac. Sci., Kyushu Univ., 7, 9–18.

VERHOOGEN, J. (1951) :   Mechanics of Ash Formation. Am. Jour. Sci., 249, 729–739.

ZINGG, Th. (1935) :   Beitrag Zur Schotteranalyse, Schweiz mineralog. Petrog. Mitt., Bd. 15, 39–140.

Suggested Additional Reading

MATSUMOTO, T. (1933) :   On the "Aira Volcano" (in Japanese), Geographical Review, Japan, 9, 614. ———— (1943) :   The four Gigantic Caldera Volcanoes of Kyushu, Jap. Jour. Geol. Geog., 19, Sp. No.

YAMAGUCHI, K. (1933) :   Petrological Study of "Ash Stone" around Bay of Kagoshima (in Japanese), Jour. Geol. Soc. Japan, 40, 377–379. ———— (1937) : Petrological Study of "Ash Stone" around the Bay of Kagoshima (part 1) (in Japanese), Jour. Geol. Soc. Japan, 44, 745. ———— (1938) : Petrological Study of the Pumice around the Bay of Kagoshima (part 3) (in Japanese), Jour. Geol. Soc. Japan, 45, 782–790. ———— (1952) : Geology of the "Shirasu" bed in Miyazaki Prefecture (in Japanese), Jour. Geol. Soc. Japan, 58, 303–304.

TANEDA, S. (1961) :   Moving of the Magma Chamber of the Sakura-jima Volcano, Jour. Geol. Soc. Japan, 67, 593–605. ———— (1978) :   Studies on the change of chemical composition of the magma of the Sakura-jima Volcano, with special reference to the upward moving of magma chamber (in Japanese), Sci. Repts. Fac. Sci., Kyushu Univ., Geol., 13, 39–46. ———— (1950) : Cordierite-bearing "Ash Stone" around the Bay of Kagoshima (in Japanese), Sci. Repts. Fac. Sci., Kyushu Univ., Geol., 2, 47–53. ———— (1975) : The shape and size of the fragments of the "Shirasu" with special reference to the collapses of the "Shirasu" cliff. (in Japanese), Sci. Repts. Shimabara Volc. Observ., 10, 9–20. ———— (1979) : Do., part 2, Ibid., 12, 1–8.
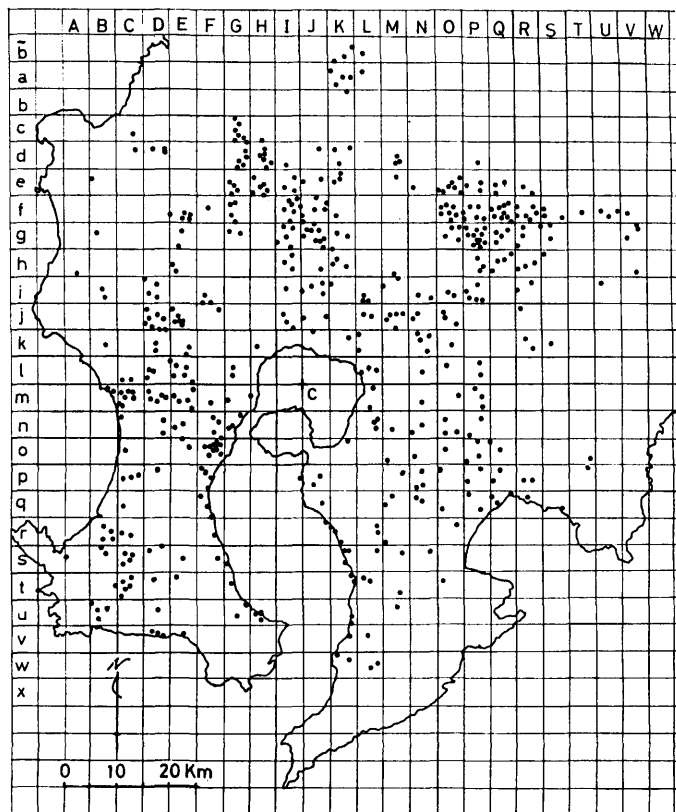
Fig. 2.3 Location of outcrops of the "Shirasu pumice flow deposits of south Kyushu, Japan where the measurements of the grain-size, grain-shape and the number of fragments per unit area at each outcrop were carried out. Median diameter analysis was also done.

Fig. 2.4 Map showing the general basement topography. (See VII. 4 in p. 118)
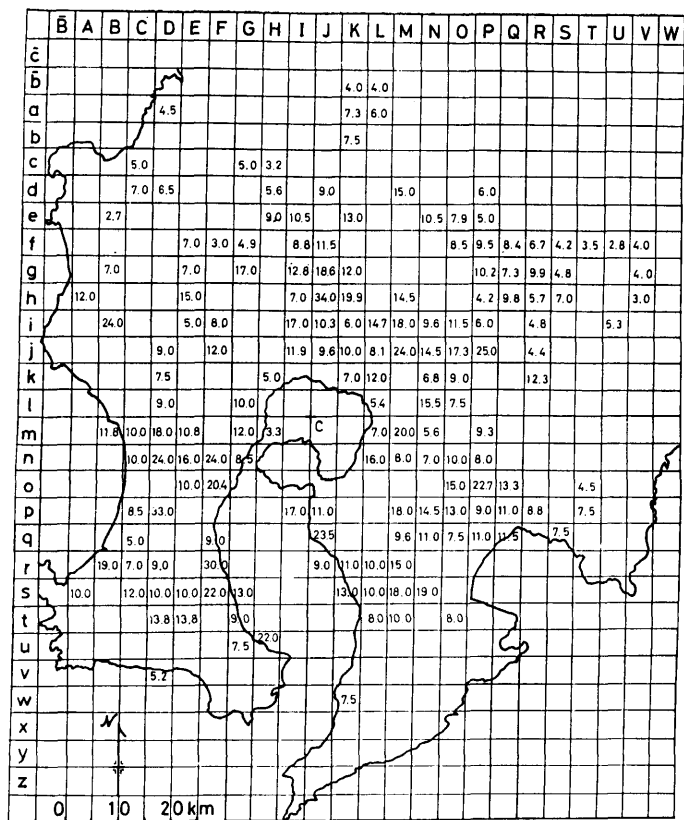C, +: Provisional center of the "Aira caldera".

Fig. 3.1.a. l_{P1} "Data map". The arithmetic means of data calculated for every squares are plotted on the map.
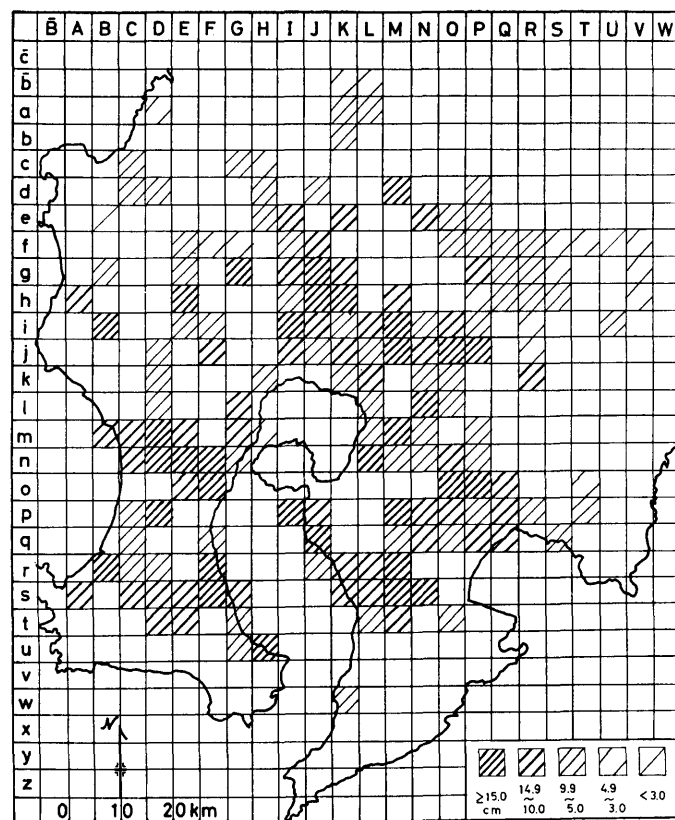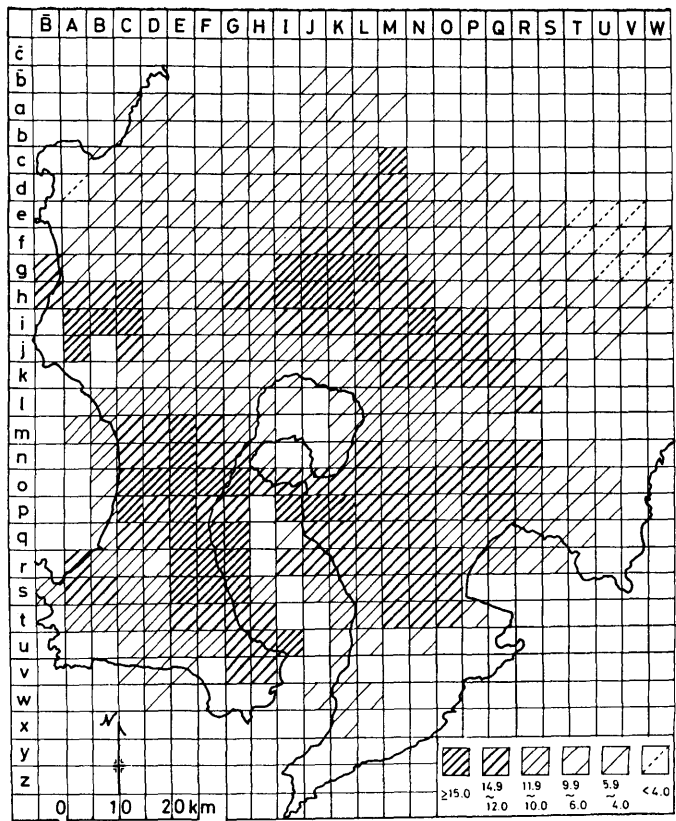
Fig. 3.1.b. l_{P1} "Hatching diagram".

≥15.0 cm   14.9~10.0   9.9~5.0   4.9~3.0   <3.0

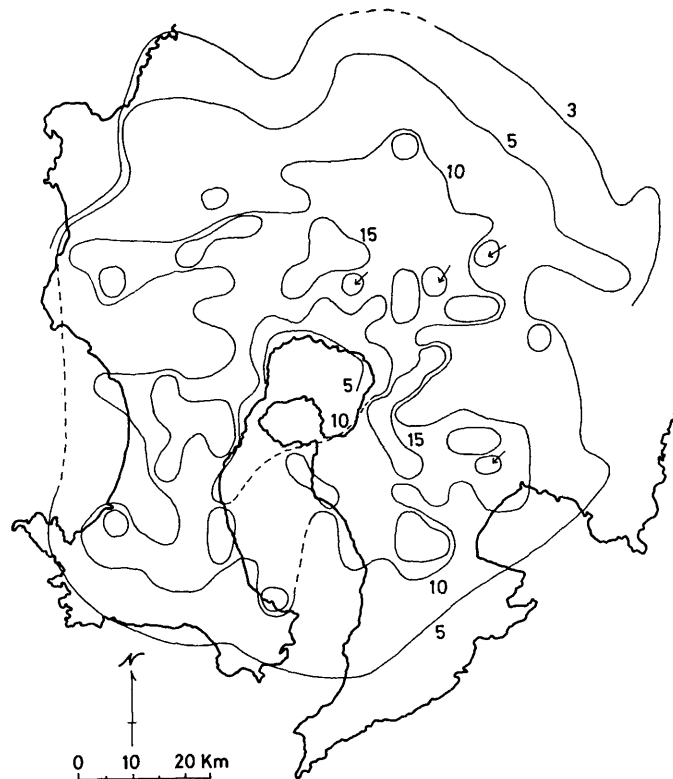Fig. 3.1.c. l$_{P1}$ "Hatching diagram", using the overlapping means.

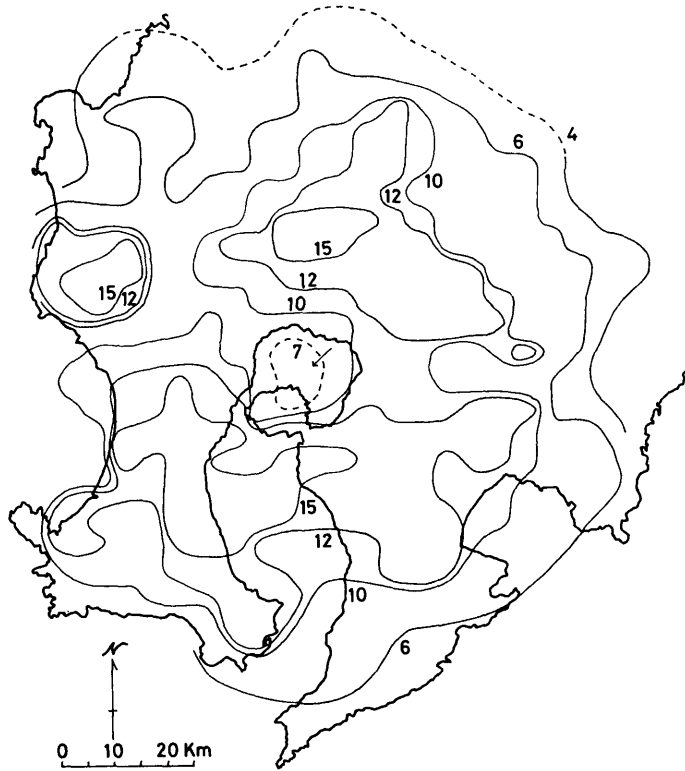Fig. 3.1.d. l$_{P1}$ "Contour lines".

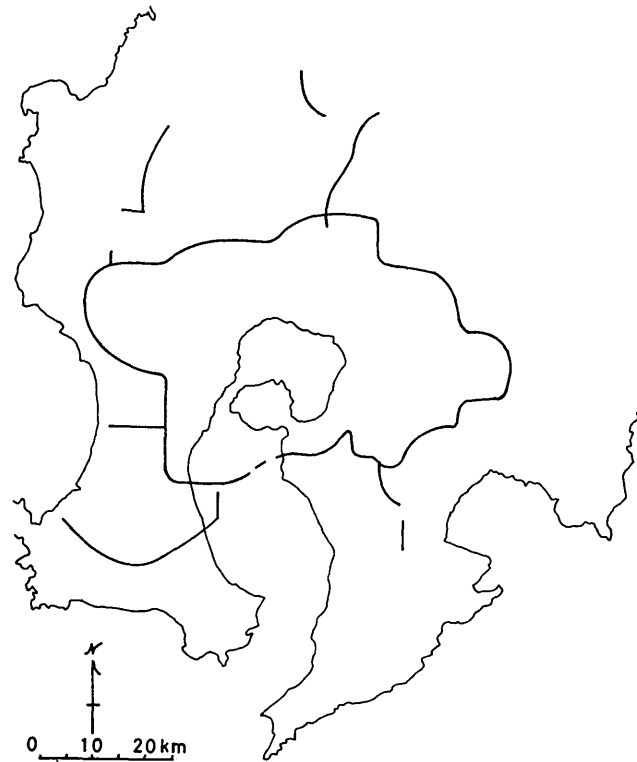Fig. 3.1.e. l$_{P1}$ "Contour lines", using the overlapping means.

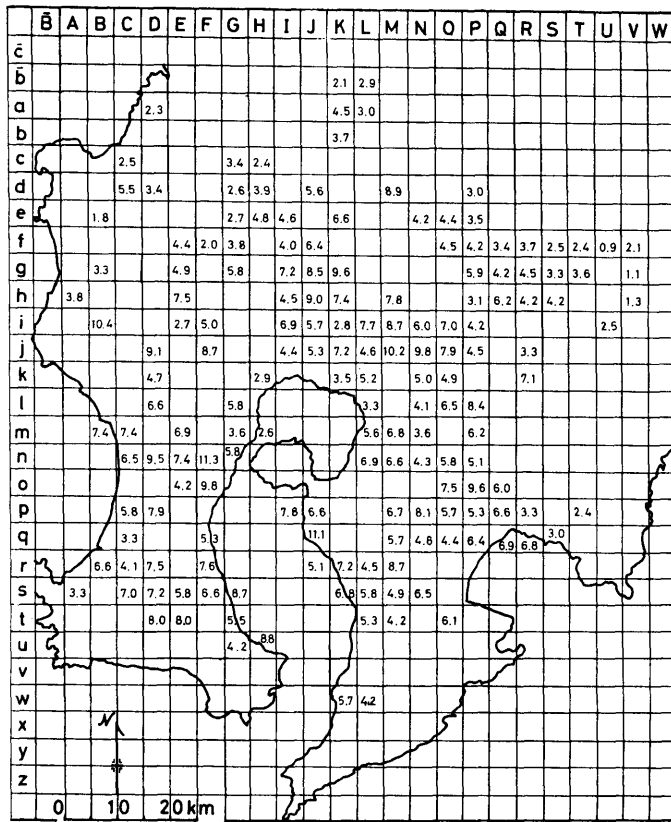Fig. 3.1.f. l$_{P1}$ "Ridge and valley lines", using the overlapping means.

Fig. 3.2.a. l_P^{av} "Data map". The arithmetic means of data calculated for every squares are plotted on a map.

Fig. 3.2.b. l_P^{av} "Hatching diagram".

Legend (Fig. 3.2.b):
≥7.0 cm | 6.9~5.0 | 4.9~3.0 | 2.9~2.0 | <2.0

Fig. 3.2.c. l_P^{av} "Hatching diagram", using the overlapping means.

Fig. 3.2.d. l_P^{av} "Contour lines".

Fig. 3.2.e. l_P^{av} "Contour lines", using the overlapping means.

Fig. 3.2.f. l_P^{av} "Ridge and velley lines", using the overlapping means.

	Ō	A	B	C	D	E	F	G	H	I	J	K	L	M	N	O	P	Q	R	S	T	U	V	W
ċ																								
b̄															0.2		3.0							
a					1.1										2.2		2.0							
b															4.0									
c				3.0																				
d				1.0	1.1				2.5		3.0			3.8			3.0							
e				3.3				2.6	2.5		2.0				1.2		4.4		1.6					
f						3.0	3.0	2.0		3.2	5.1						4.5	1.8	2.4	1.2	1.1	1.3	0.4	0.5
g			1.9		4.0				6.0	3.4	3.3						2.0	1.8	1.4	1.2				1.3
h	1.5				2.0				6.0	10.0	3.0			4.4				1.1	1.6	1.6	1.9			
i			2.2		8.0	5.8			9.0	6.4	5.7	4.3	5.0	3.1	1.8	3.9			0.7			2.7		
j				6.0		6.0			11.7	4.2	12.0	2.2	3.9	4.1	2.8	3.0			1.0					
k				4.2				2.0			2.0	3.5			4.5	2.0				4.6				
l				2.0			7.0			6.7			3.4	6.5	1.0									
m			2.2	3.5		3.0		6.0	3.6			5.0	7.0	3.3				1.7						
n					1.3	4.0	2.0	5.7	4.8			5.0	4.0	3.0	3.3	1.5								
o						2.0	8.4								4.0	1.8	1.5			1.5				
p				3.7	6.0				21.0	1.5			2.2	1.5	3.0	2.0	2.0	1.8		1.5				
q				1.0			3.1		6.0				13.0	3.3	1.5	2.9			1.0		2.2			
r			2.5	1.6	2.5		4.0		5.0	4.5	1.8	5.0												
s	5.0			5.5	2.5	4.0	4.0	5.0		3.8	1.0	2.9	6.0											
t					2.3	2.3		5.0				1.2	1.5		1.2									
u							3.5	2.5																
v					1.3																			
w									1.0															
x				N																				
y																								
z			0	10	20 km																			

Fig. 3.3.a. l$_{L1}$ "Data map". The arithmetic means of data calculated for every squares are plotted on a map.

Legend: ≥10.0 cm | 9.9~6.0 | 5.9~4.0 | 3.9~3.0 | 2.9~2.0 | <2.0
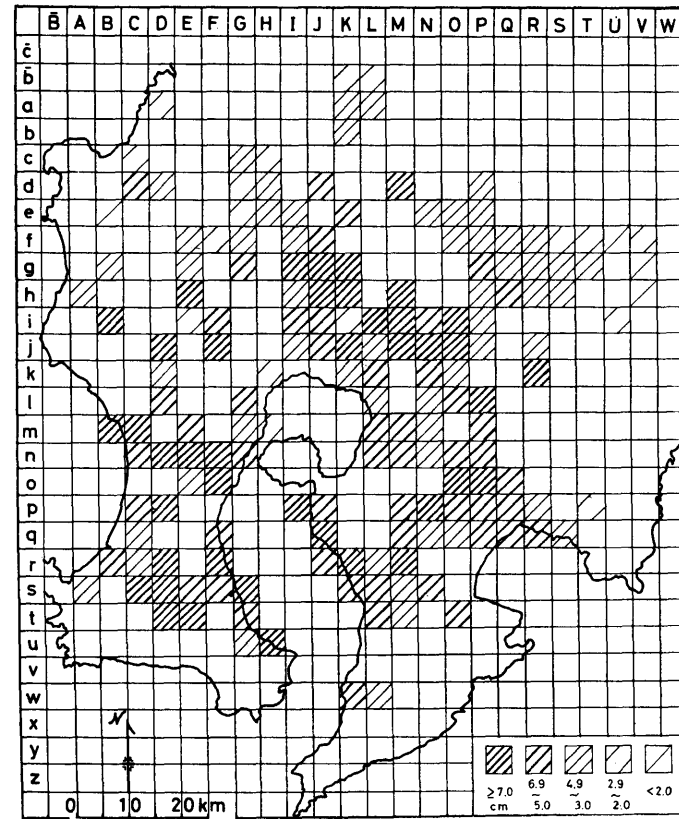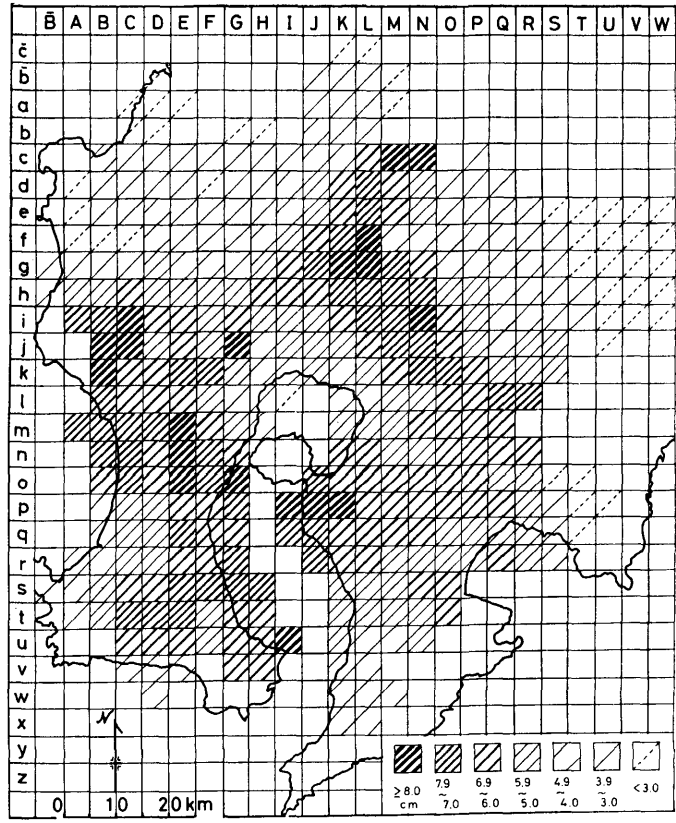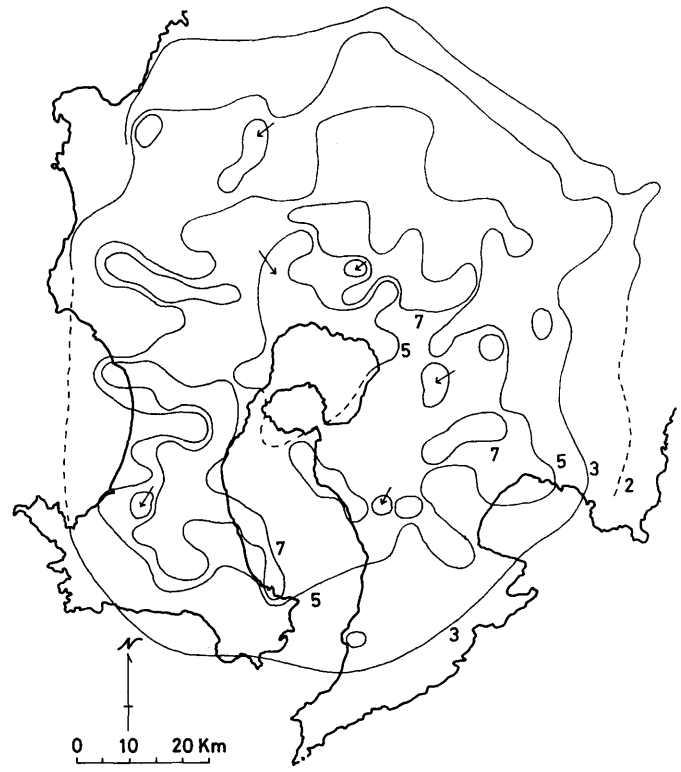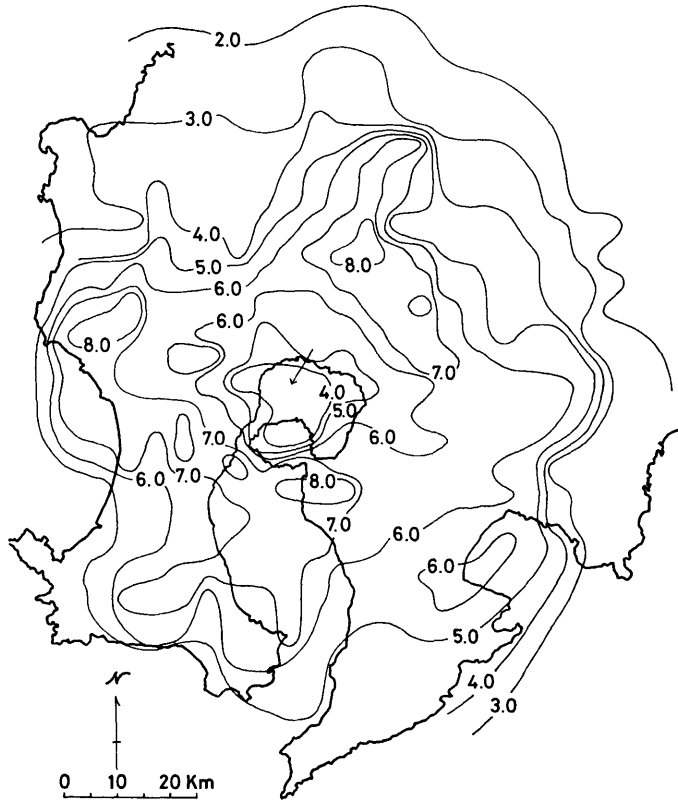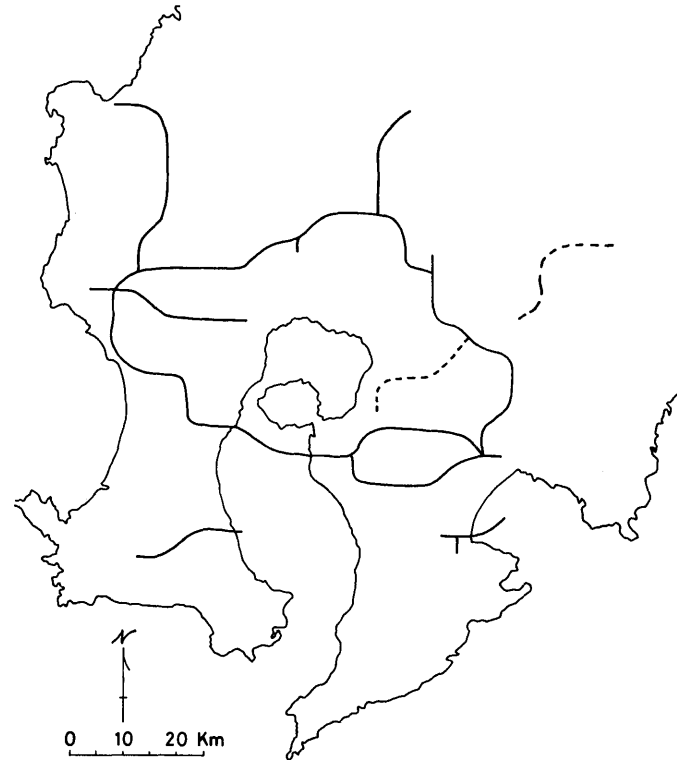
Fig. 3.3.b. l$_{L1}$ "Hatching diagram".

Fig. 3.3.c. l_{L1} "Hatching diagram", using the overlapping means.

Fig. 3.3.d. l_{L1} "Contour lines".

Fig. 3.3.e. l_{L1} "Contour lines", using the overlapping
means.

Fig. 3.3.f. l_{L1} "Ridge and valley lines", using the
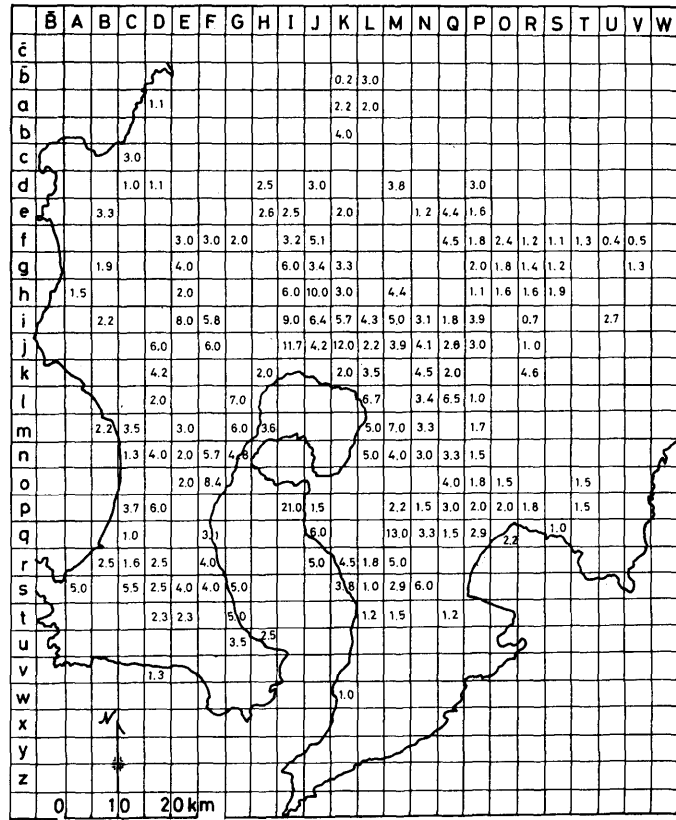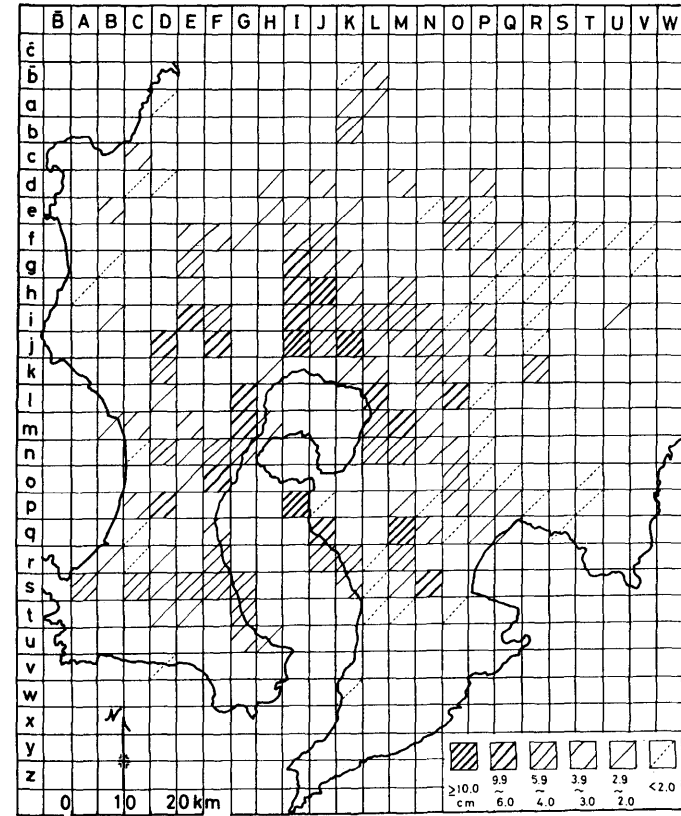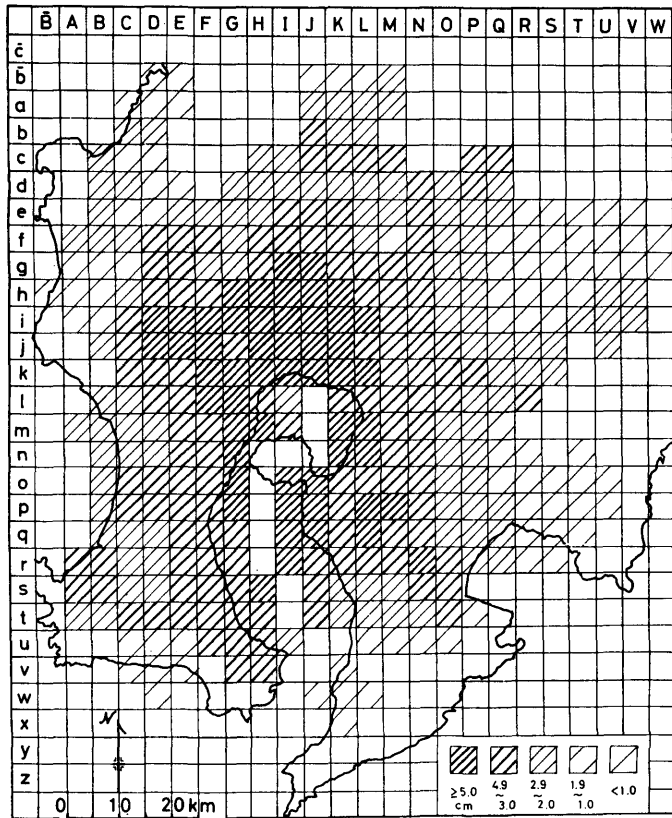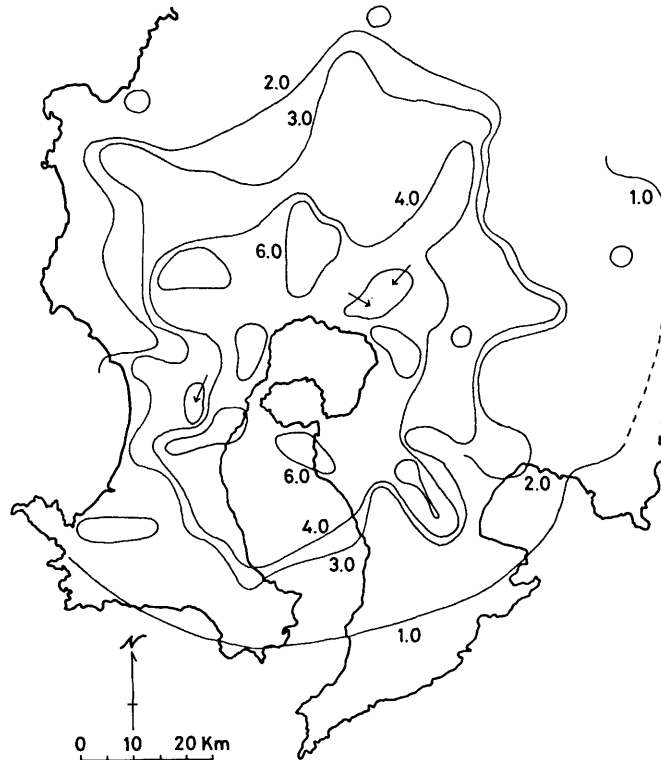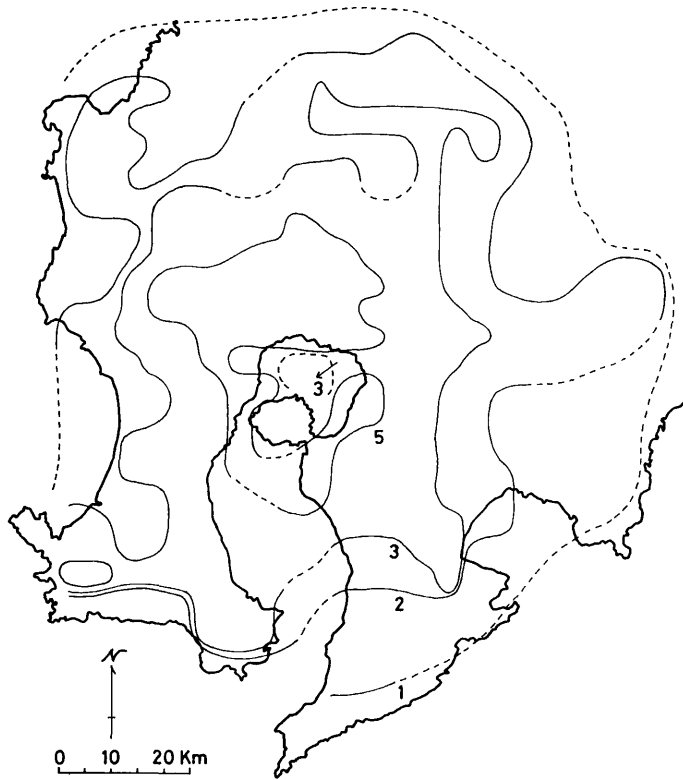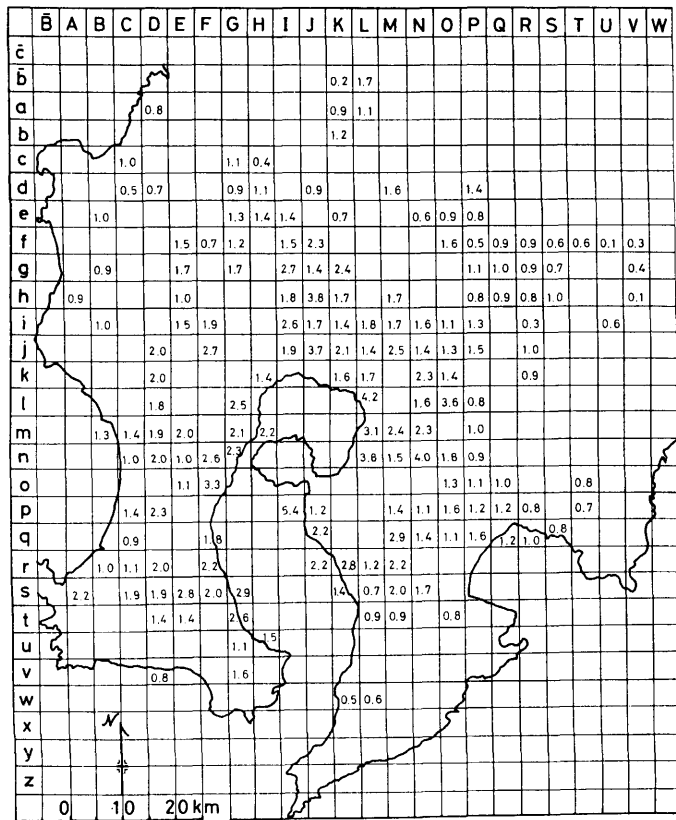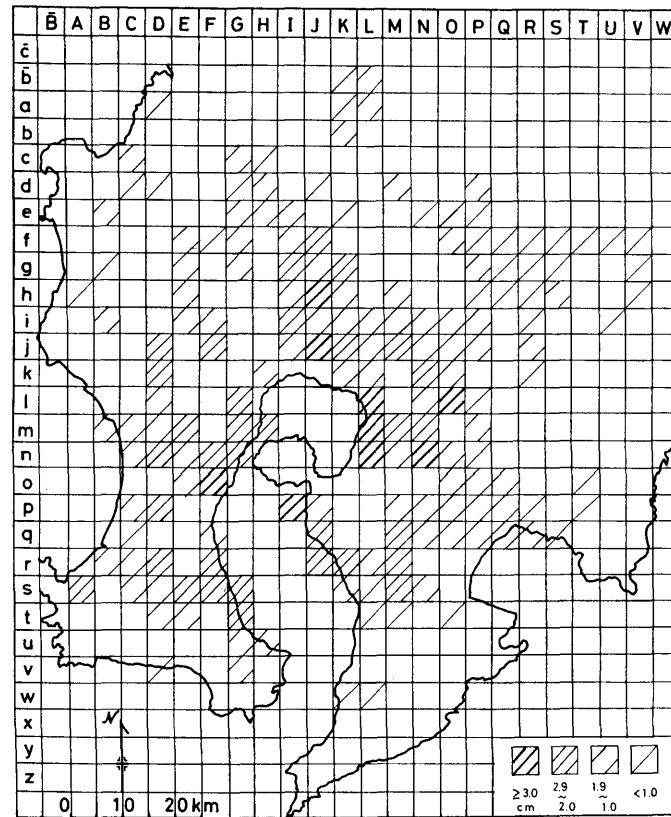overlapping means.

Fig. 3.4.a. l_L^{av} "Data map". — grid columns B̄, A, B, C, D, E, F, G, H, I, J, K, L, M, N, O, P, Q, R, S, T, U, V, W; grid rows c̄, b̄, a, b, c, d, e, f, g, h, i, j, k, l, m, n, o, p, q, r, s, t, u, v, w, x, y, z.

row	B̄	A	B	C	D	E	F	G	H	I	J	K	L	M	N	O	P	Q	R	S	T	U	V	W
b̄												0.2	1.7											
a					0.8							0.9	1.1											
b												1.2												
c				1.0				1.1	0.4															
d				0.5	0.7			0.9	1.1		0.9			1.6			1.4							
e				1.0				1.3	1.4		0.7					0.6	0.9	0.8						
f							1.5	0.7	1.2		1.5	2.3				1.6	0.5	0.9	0.9	0.6	0.6	0.1	0.3	
g			0.9				1.7		1.7		2.7	1.4	2.4				1.1	1.0	0.9	0.7				0.4
h	0.9						1.0				1.8	3.8	1.7		1.7		0.8	0.9	0.8	1.0				0.1
i			1.0				1.5	1.9			2.6	1.7	1.4	1.8	1.7	1.6	1.1	1.3		0.3		0.6		
j					2.0		2.7				1.9	3.7	2.1	1.4	2.5	1.4	1.3	1.5		1.0				
k					2.0					1.4		1.6	1.7		2.3	1.4		0.9						
l					1.8			2.5					4.2		1.6	3.6	0.8							
m			1.3	1.4	1.9	2.0		2.1	2.2				3.1	2.4	2.3		1.0							
n				1.0	2.0	1.0	2.6	2.3					3.8	1.5	4.0	1.8	0.9							
o							1.1	3.3							1.3	1.1	1.0		0.8					
p					1.4	2.3				5.4	1.2		1.4	1.1	1.6	1.2	1.2	0.8		0.7				
q					0.9			1.8		2.2			2.9	1.4	1.1	1.6		1.2	1.0	0.8				
r				1.0	1.1	2.0		2.2		2.2	2.8	1.2	2.2											
s		2.2		1.9	1.9	2.8	2.0	2.9			1.4		0.7	2.0	1.7									
t					1.4	1.4		2.6				0.9	0.9		0.8									
u								1.1	1.5															
v					0.8			1.6																
w												0.5	0.6											

0 10 20 km

Fig. 3.4.a. l_L^{av} "Data map". The arithmetic means of data calculated for every squares are plotted on a map.
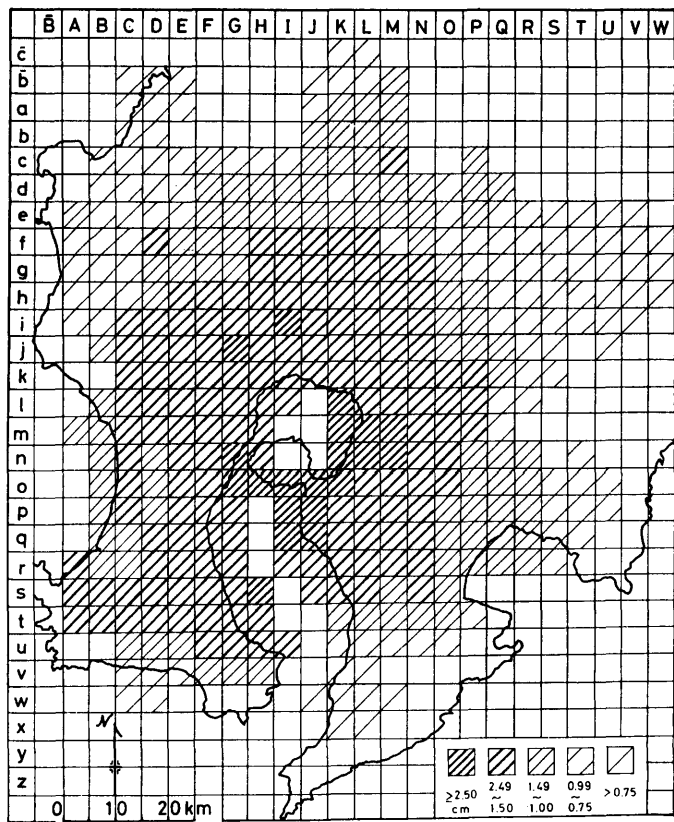
Fig. 3.4.b. l_L^{av} "Hatching diagram".

Legend: ≥3.0 cm | 2.9~2.0 | 1.9~1.0 | <1.0

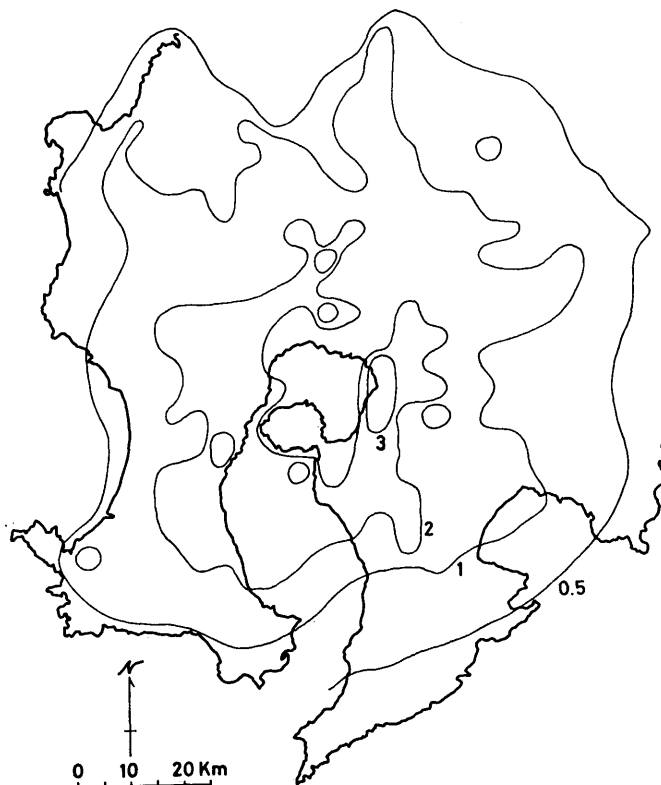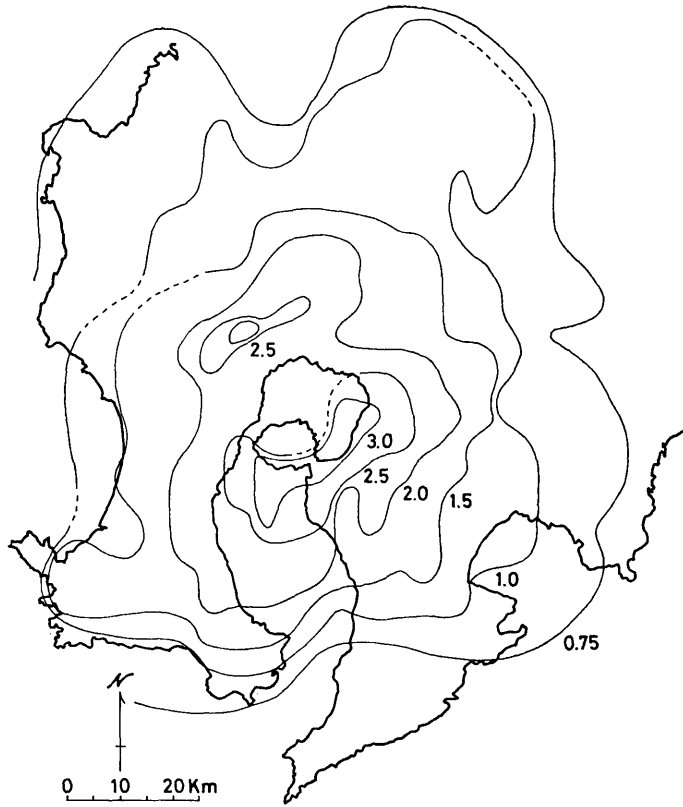Fig. 3.4.c. l_L^{av} "Hatching diagram", using the overlapping means.

Fig. 3.4.d. l_L^{av} "Contour lines".

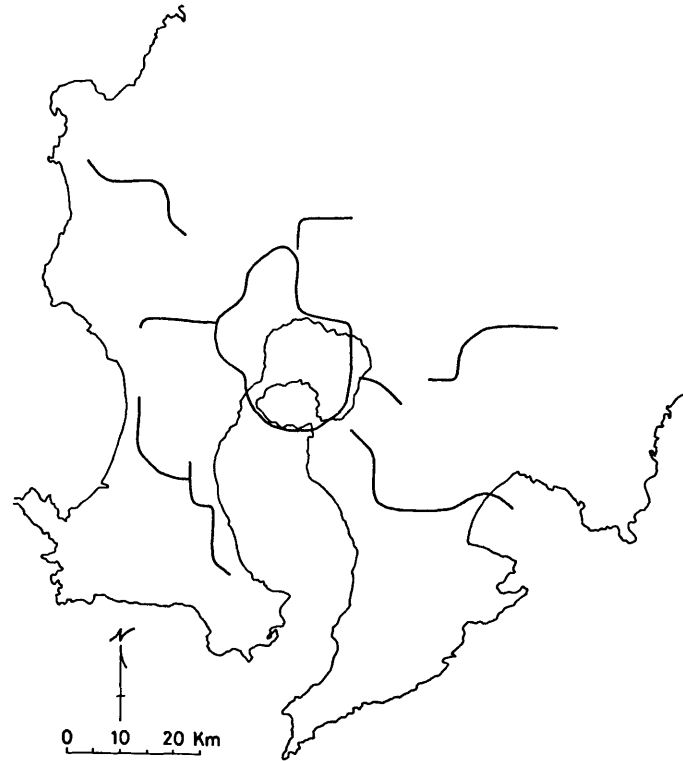Fig. 3.4.e. l_L^{av} "Contour lines", using the overlapping means.

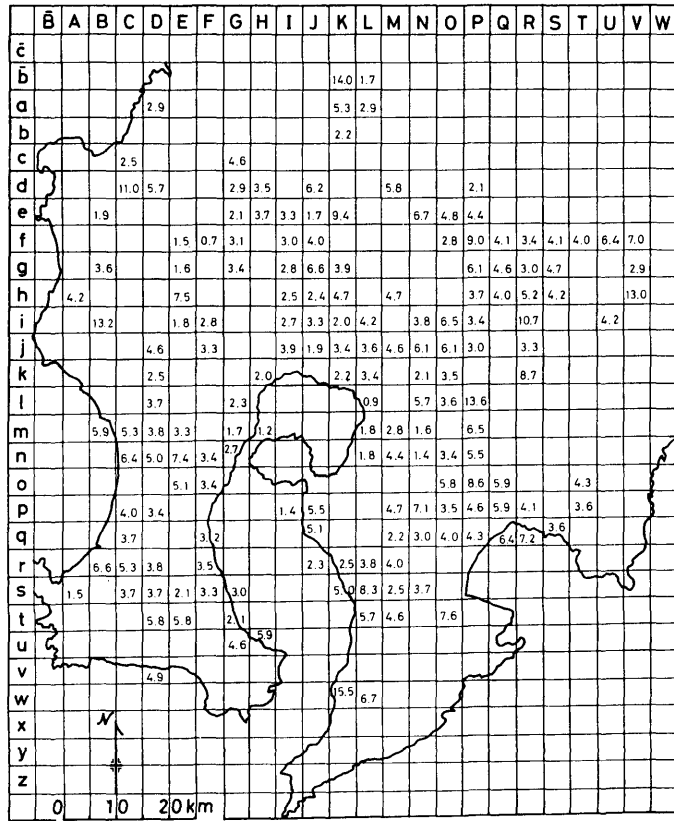Fig. 3.4.f. l_L^{av} "Ridge and valley lines", using the overlapping means.

Fig. 3.5.a. l_P^{av}/l_L^{av} "Data map". The arithmetic means of data calculated for every squares are plotted on a map.
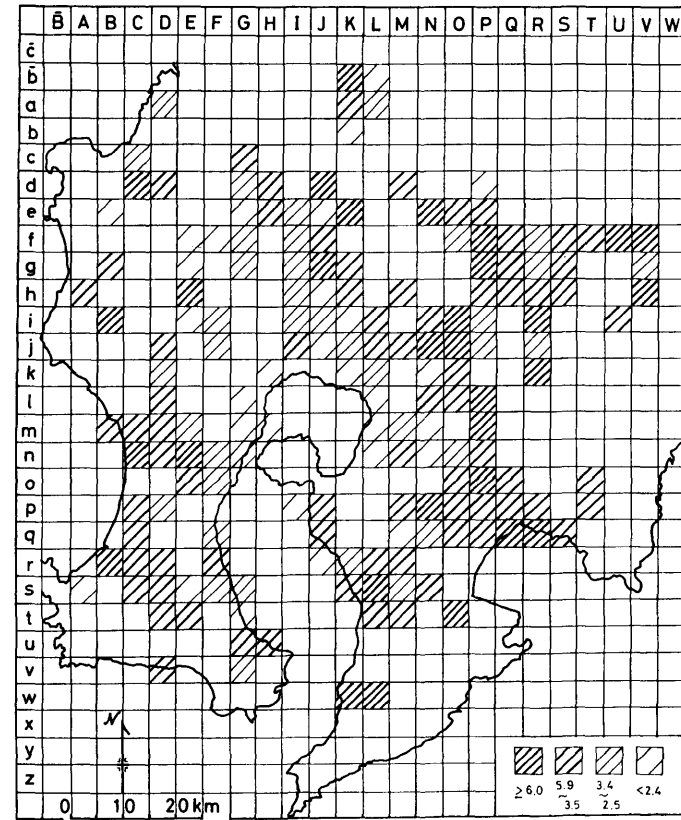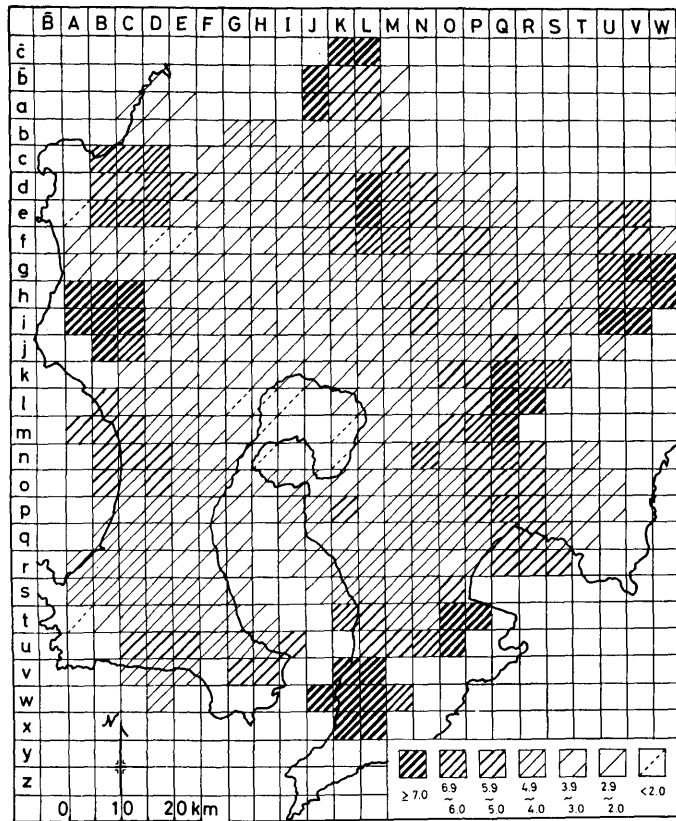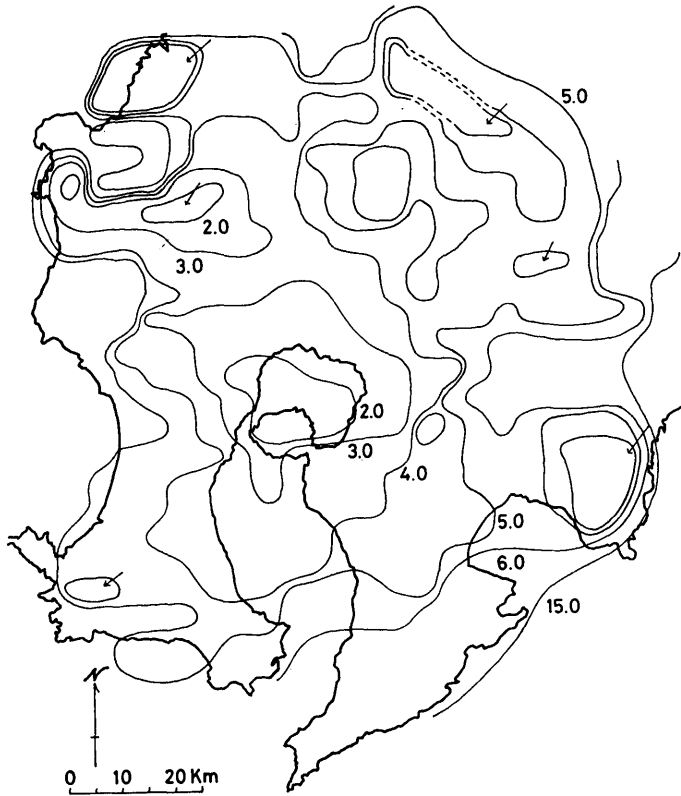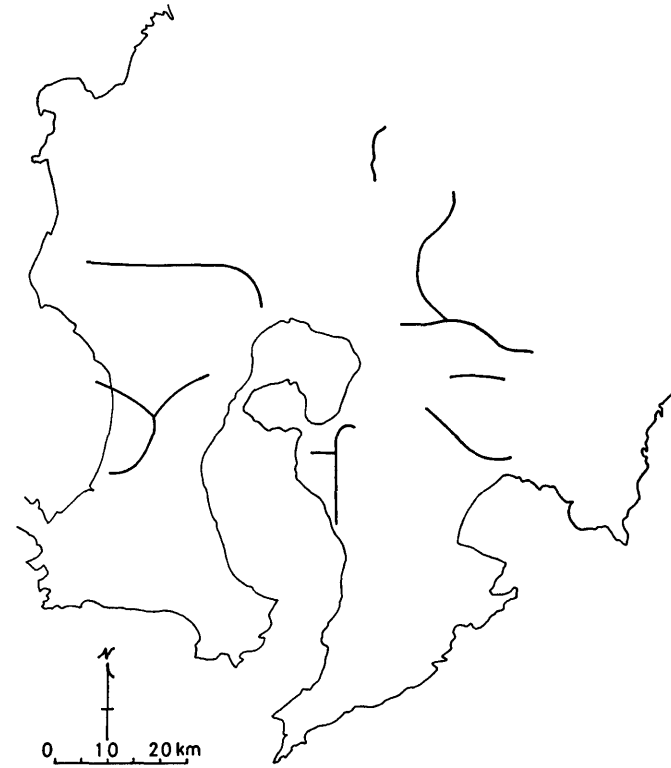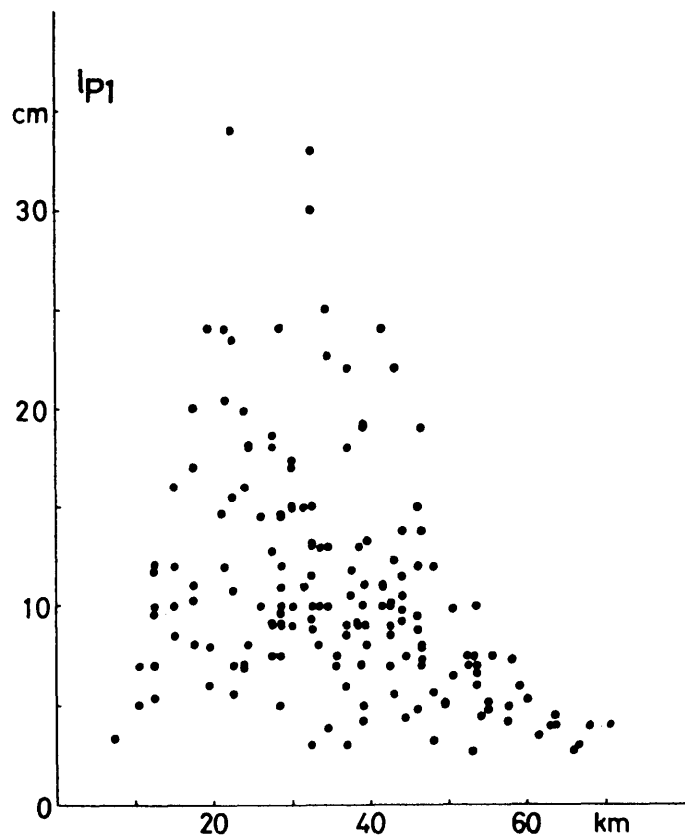
Fig. 3.5.b. l_P^{av}/l_L^{av} "Hatching diagram".

Fig. 3.5.c. l_P^{va}/l_L^{av} "Hatching diagram", using the overlapping means.
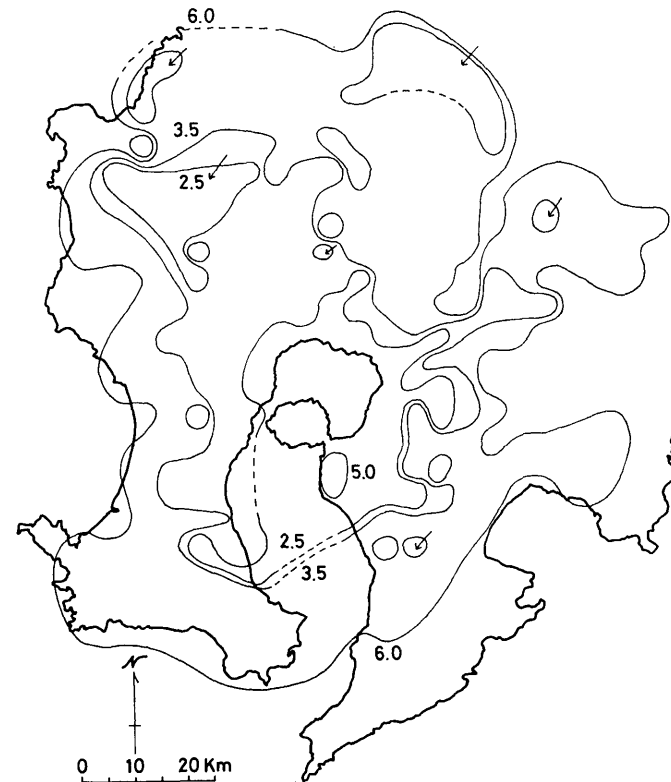
Fig. 3.5.d. l_P^{av}/l_L^{av} "Contour lines".

Fig. 3.5.e. l_P^{av}/l_L^{av} "Contour lines", using the overlapping means.

Fig. 3.5.f. l_P^{av}/l_L^{av} "Ridge and valley lines", using the overlapping means.

Fig. 3.6.a. Plot of l_{P1} vs. D (the distance from the source in km.)
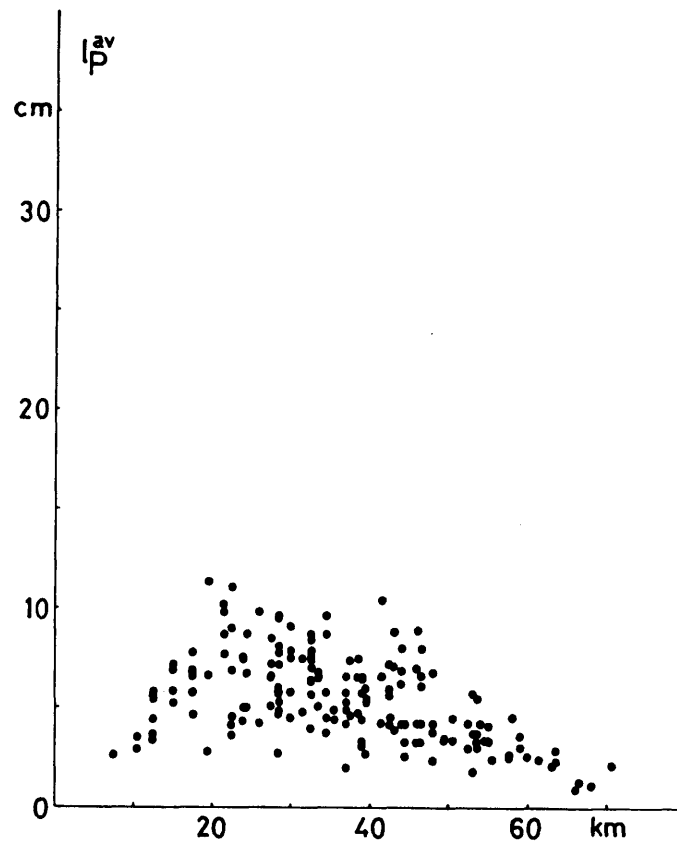
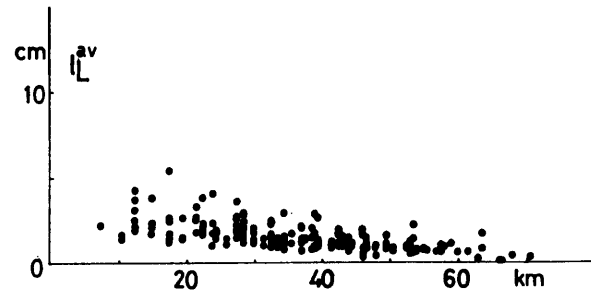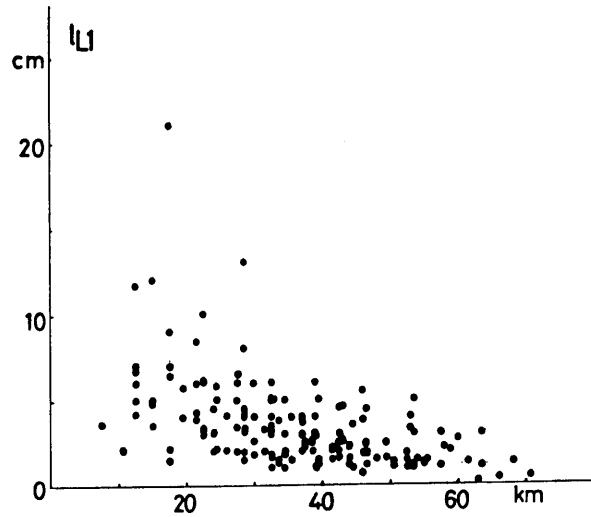Fig. 3.6.b. Plot of l_P^{av} vs. D (km.)

Fig. 3.6.c. Plot of l_{L1} vs. D (km.)
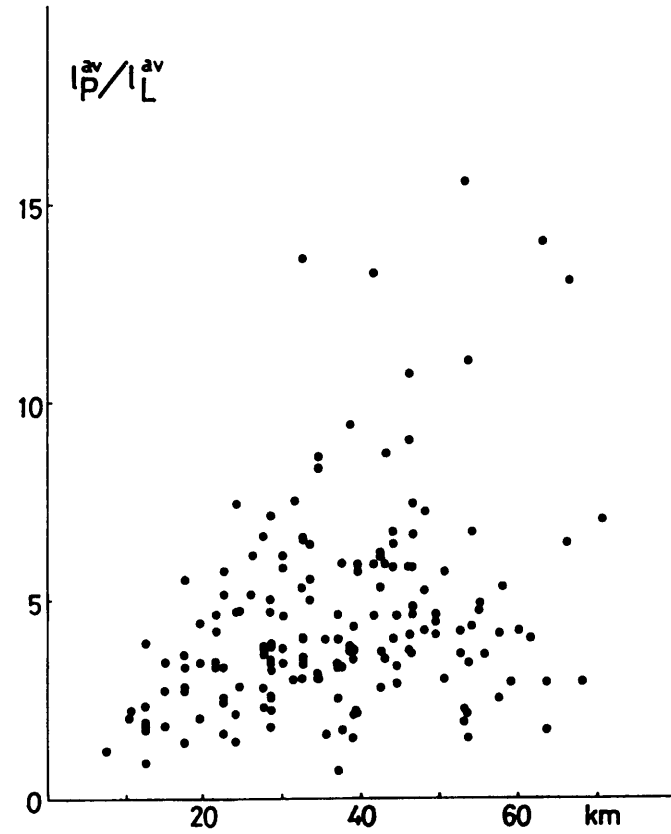
Fig. 3.6.d. Plot of l_L^{av} vs. D (km.)

Fig. 3.6.e. Plot of l_P^{av}/l_L^{av} vs. D (km.)
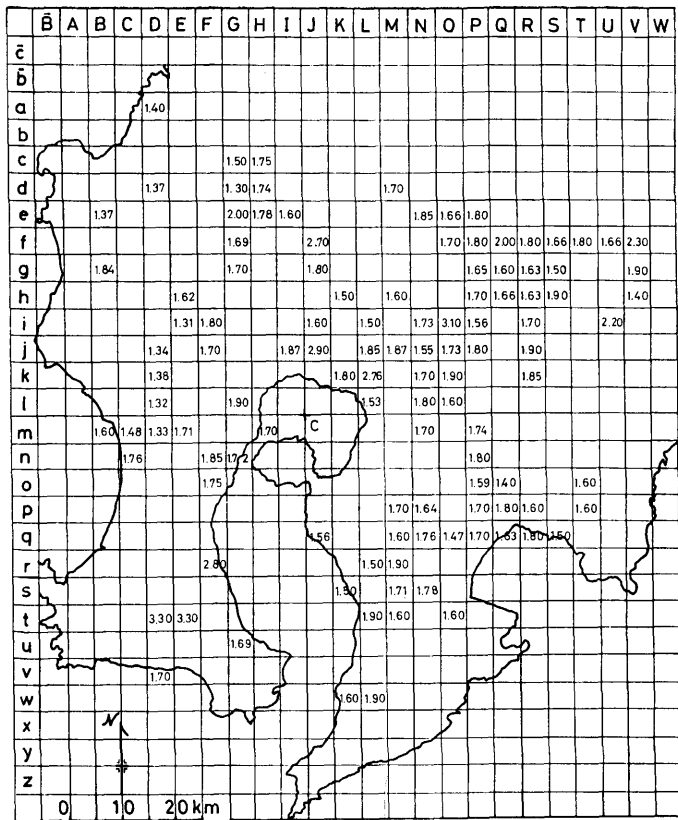
Fig. 4.1.a. l_P^{av}/s_P^{av} "Data map". The arithmetic means of data calculated for every squares are plotted on a map.
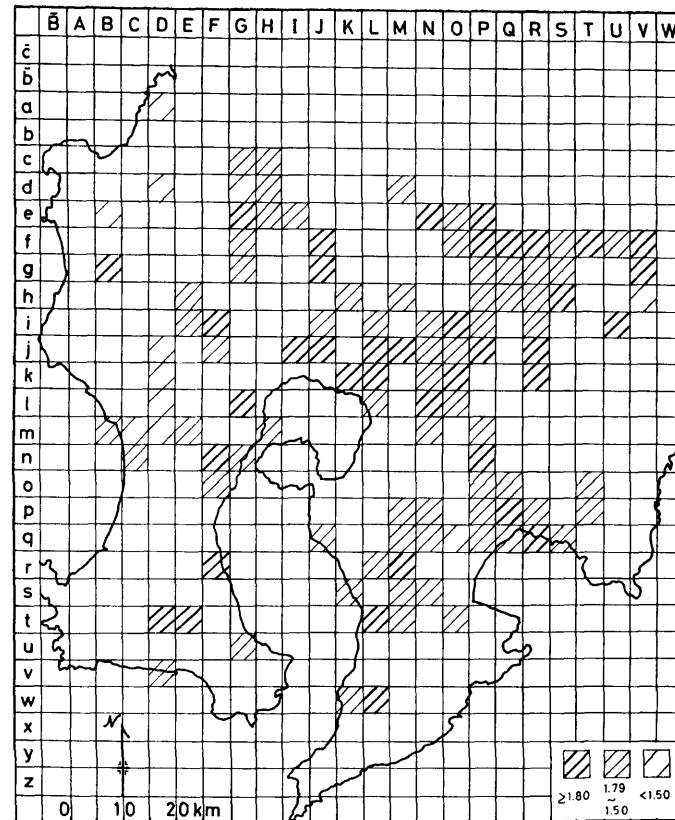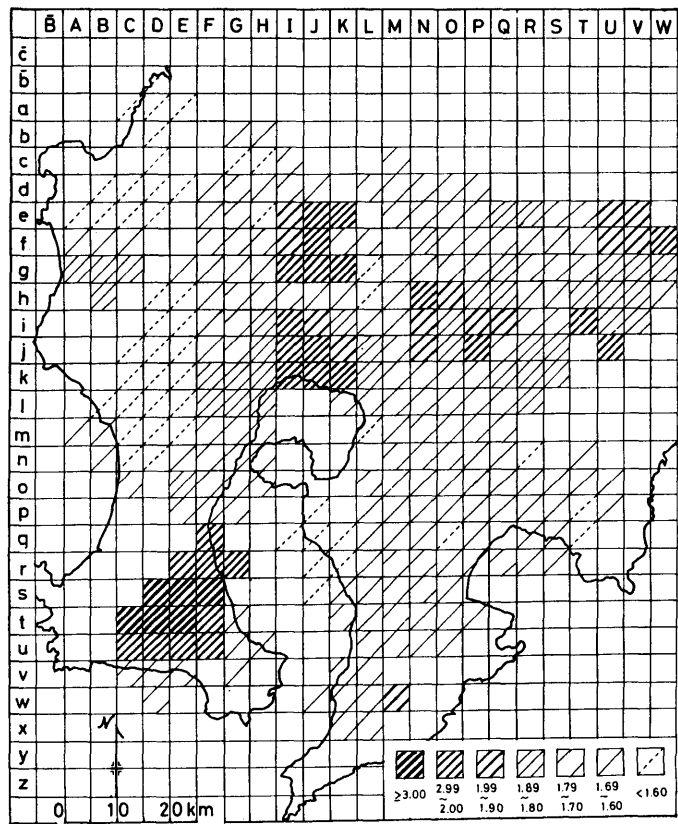
Fig. 4.1.b. l_P^{av}/s_P^{av} "Hatching diagram".

Legend (Fig. 4.1.b): ≥1.80 | 1.79–1.50 | <1.50

Scale: 0 10 20 km

Data map (Fig. 4.1.a) values:

Row	Values
a	D=1.40
c	F=1.50, G=1.75
d	C=1.37, F=1.30, G=1.74, J=1.70
e	A=1.37, F=2.00, G=1.78, H=1.60, M=1.85, N=1.66, O=1.80
f	F=1.69, H=2.70, O=1.70, P=1.80, Q=2.00, R=1.80, S=1.66, T=1.80, U=1.66, V=2.30
g	A=1.84, F=1.70, H=1.80, P=1.65, Q=1.60, R=1.63, S=1.50, V=1.90
h	D=1.62, I=1.50, K=1.60, P=1.70, Q=1.66, R=1.63, S=1.90, V=1.40
i	C=1.31, D=1.80, G=1.60, I=1.50, K=1.73, L=3.10, M=1.56, O=1.70, U=2.20
j	C=1.34, E=1.70, H=1.87, I=2.90, K=1.85, L=1.87, M=1.55, N=1.73, O=1.80, Q=1.90
k	C=1.38, H=1.80, I=2.76, K=1.70, L=1.90, O=1.85
l	C=1.32, E=1.90, J=1.53, L=1.80, M=1.60
m	A=1.60, B=1.48, C=1.33, D=1.71, F=1.70, L=1.70, N=1.74
n	B=1.76, E=1.85, F=1.72, N=1.80
o	E=1.75, N=1.59, O=1.40, Q=1.60
p	J=1.70, K=1.64, N=1.70, O=1.80, P=1.60, R=1.60
q	G=1.56, K=1.60, L=1.76, M=1.47, N=1.70, O=1.63, P=1.80, Q=1.50
r	E=2.80, K=1.50, L=1.90
s	K=1.30, M=1.71, N=1.78
t	D=3.30, E=3.30, K=1.90, L=1.60, N=1.60
u	E=1.69
v	D=1.70
w	K=1.60, L=1.90

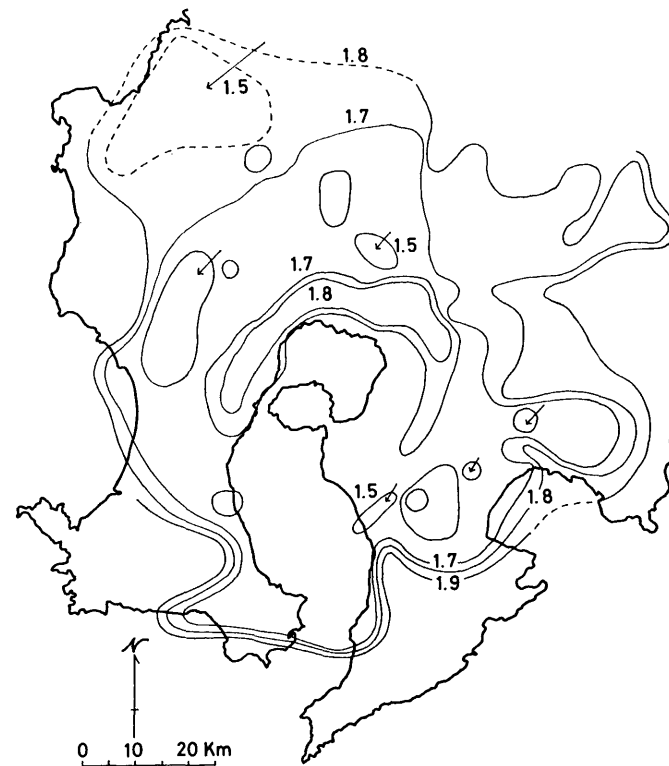Fig. 4.1.c. l_P^{av}/s_P^{av} "Hatching diagram", using the overlapping means.

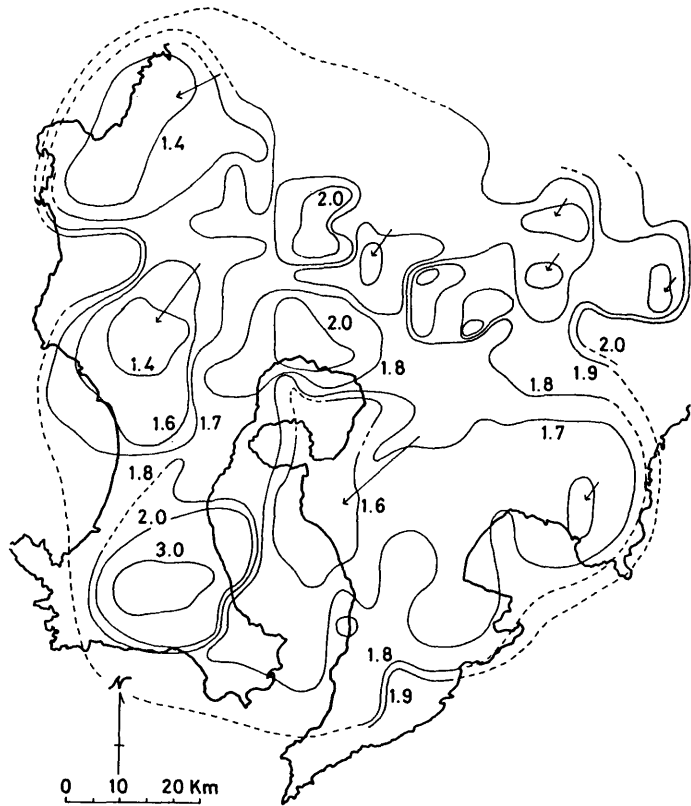Fig. 4.1.d. l_P^{av}/s_P^{av} "Contour lines".

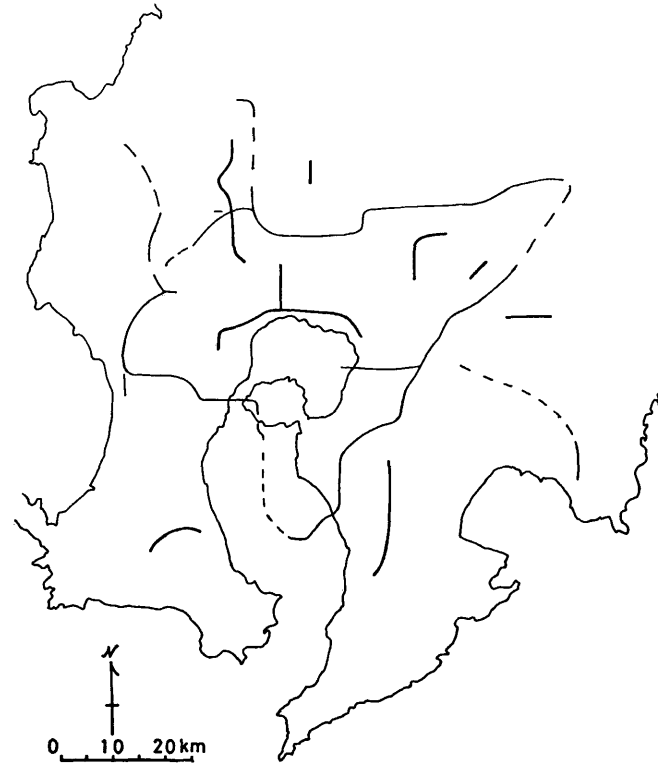Fig. 4.1.e. l_P^{av}/s_P^{av} "Contour lines", using the overlapping means.

Fig. 4.1.f. l_P^{av}/s_P^{av} "Ridge and valley lines", using the overlapping means.
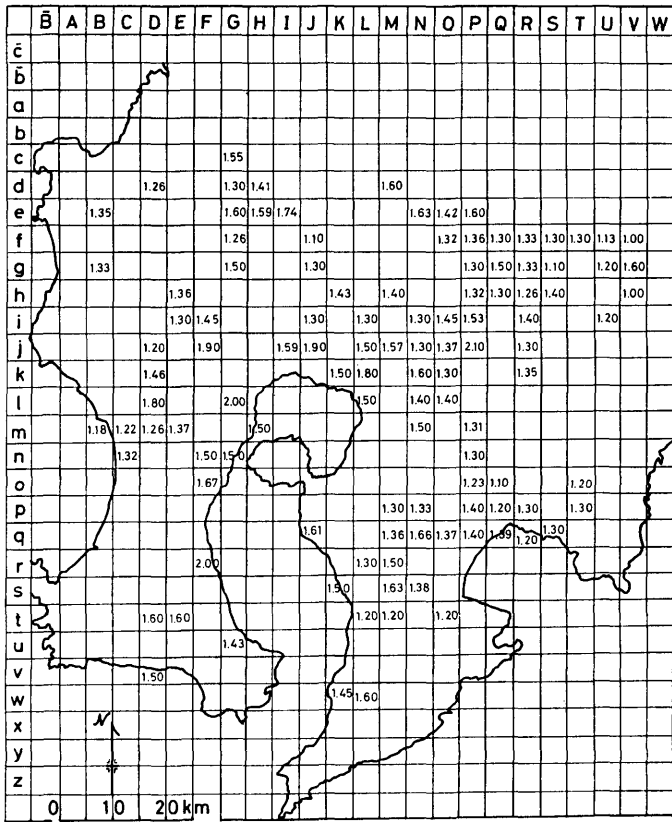
Fig. 4.2.a.

	B̄	A	B	C	D	E	F	G	H	I	J	K	L	M	N	O	P	Q	R	S	T	U	V	W
c̄																								
b̄																								
a																								
b																								
c								1.55																
d					1.26			1.30	1.41						1.60									
e			1.35					1.60	1.59	1.74				1.63	1.42	1.60								
f							1.26			1.10					1.32	1.36	1.30	1.33	1.30	1.30	1.13	1.00		
g			1.33				1.50			1.30					1.30	1.50	1.33	1.10			1.20	1.60		
h					1.36					1.43		1.40		1.32	1.30	1.26	1.40					1.00		
i					1.30	1.45			1.30		1.30		1.30	1.45	1.53		1.40			1.20				
j					1.20		1.90			1.59	1.90		1.50	1.57	1.30	1.37	2.10		1.30					
k					1.46								1.50	1.80		1.60	1.30		1.35					
l					1.80		2.00						1.50		1.40	1.40								
m		1.18	1.22	1.26	1.37		1.50							1.50		1.31								
n				1.32			1.50	1.50							1.30									
o							1.67							1.23	1.10		1.20							
p											1.30	1.33		1.40	1.20	1.30		1.30						
q									1.61			1.36	1.66	1.37	1.40	1.39	1.20	1.30						
r						2.00						1.30	1.50											
s											1.90		1.63	1.38										
t					1.60	1.60						1.20	1.20		1.20									
u							1.43																	
v					1.50																			
w											1.45	1.60											
x																								
y																								
z																								

0   10   20 km

Fig. 4.2.a. l_L^{av}/s_L^{av} "Data map". The arithmetic means of data calculated for every square are plotted on a map.

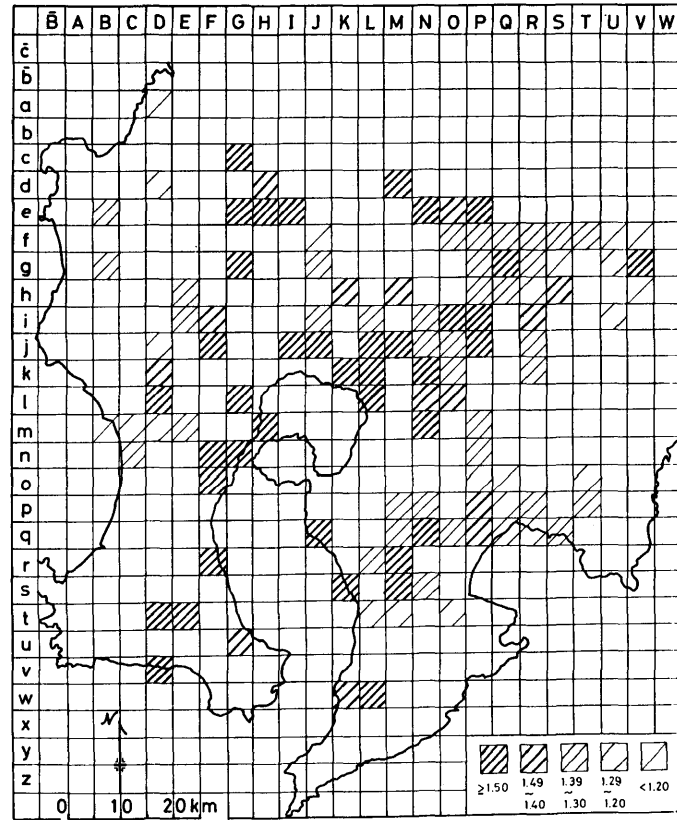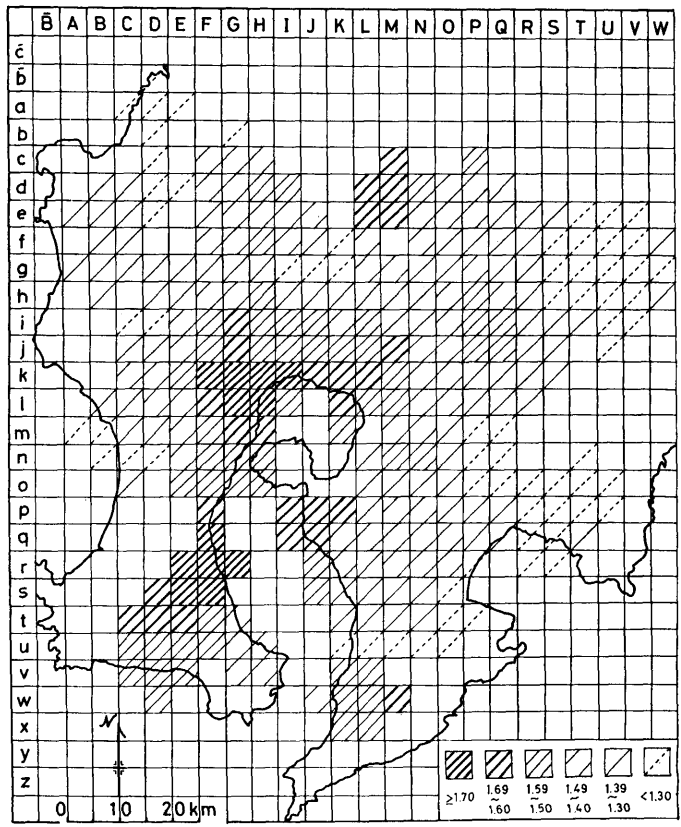Fig. 4.2.b. l_L^{av}/s_L^{av} "Hatching diagram".

Legend: ≥1.50 | 1.49–1.40 | 1.39–1.30 | 1.29–1.20 | <1.20

Fig. 4.2.c. l_L^{av}/s_L^{av} "Hatching diagram", using the overlapping means.
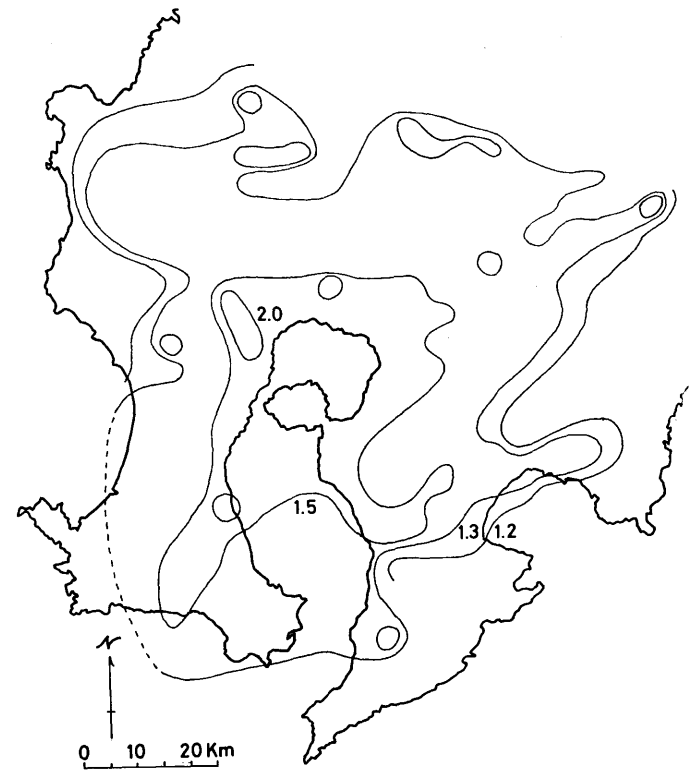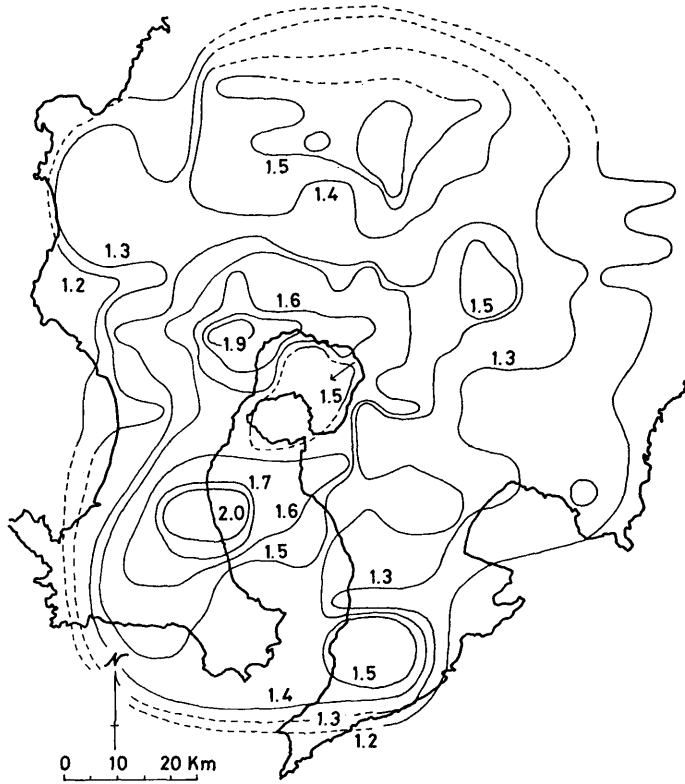

Fig. 4.2.d. l_L^{av}/s_L^{av} "Contour lines".

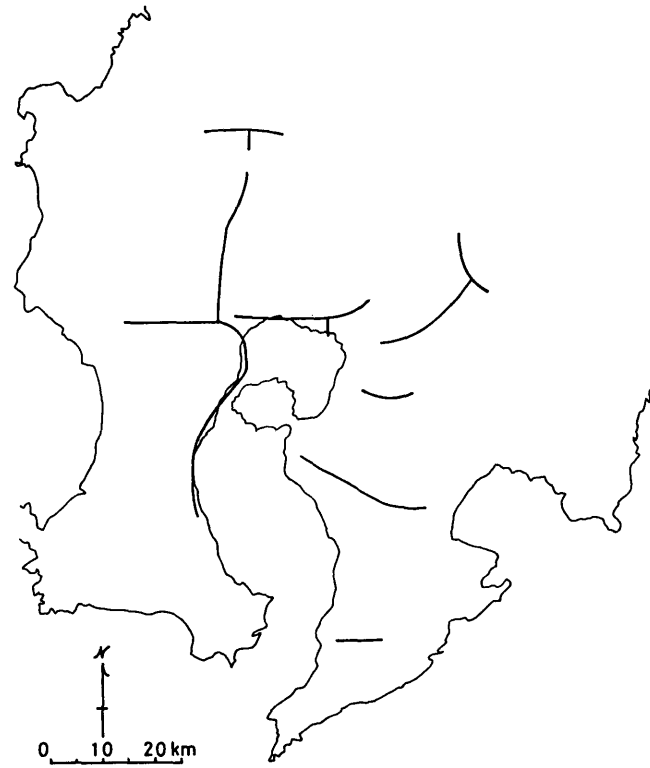Fig. 4.2.e. l_L^{av}/s_L^{av} "Contour lines", using the overlapping means.

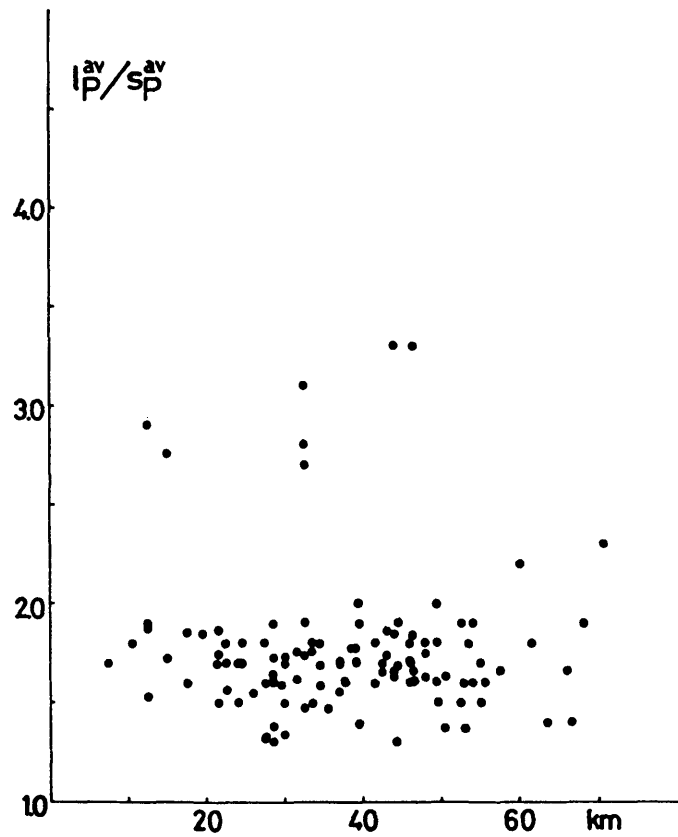Fig. 4.2.f. l_L^{av}/s_L^{av} "Ridge and valley lines", using the overlapping means.

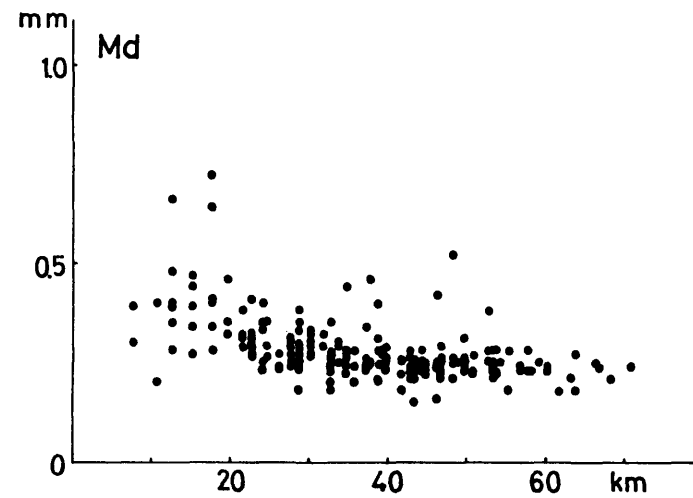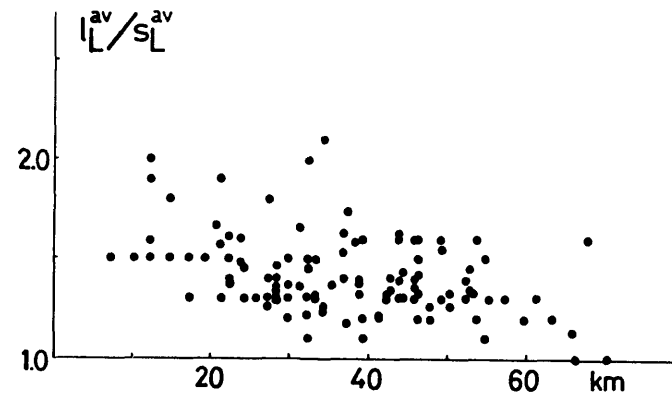Fig. 4.3.a. Plot of l_P^{av}/s_P^{av} vs. D (km.)

Fig. 4.3.b. Plot of l_L^{av}/s_L^{av} vs. D (km.)
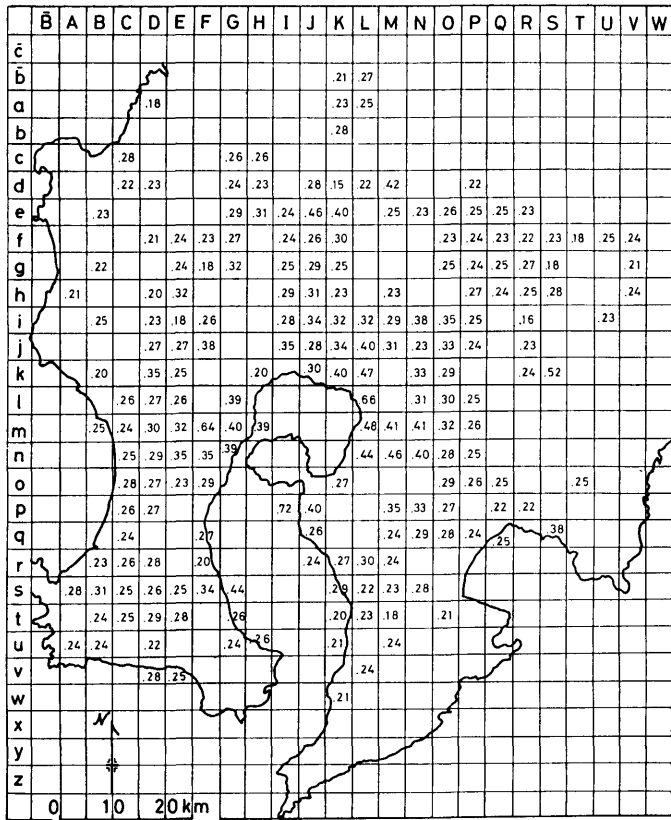
Fig. 5.2. Plot of Md vs. D (km.)

Fig. 5.1.a. Md "Data map". The arithmetic means of data calculated for every squares are plotted on a map.
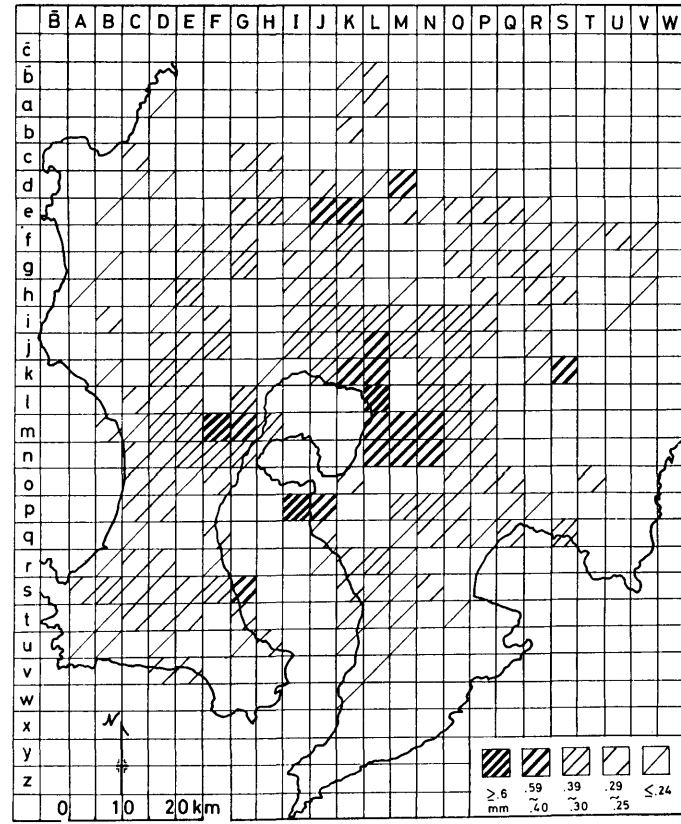
Eig. 5.1.b. Md "Hatching diagram".
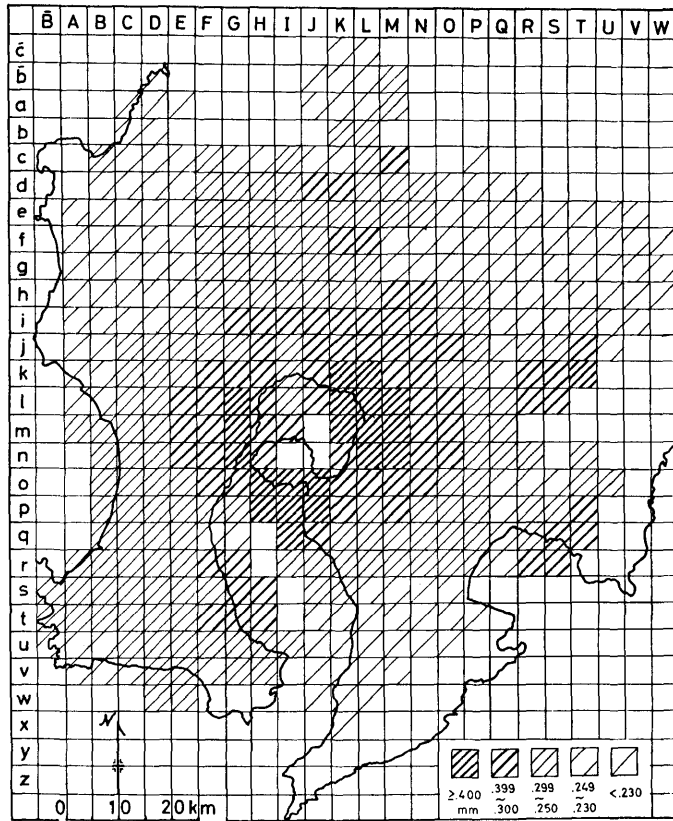
Fig. 5.1.c.   Md "Hatching diagram", using overlapping means.
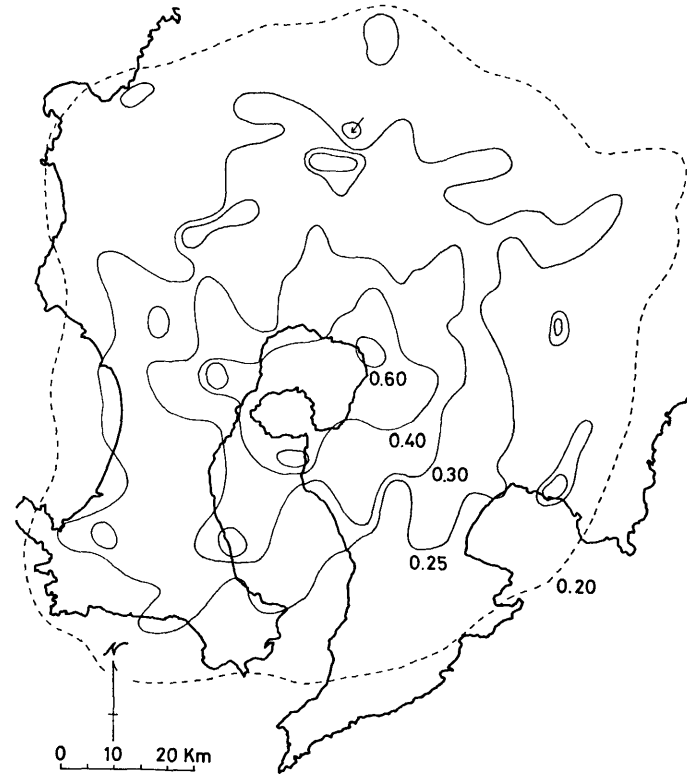
Fig. 5.1.d.   Md "Contour lines".

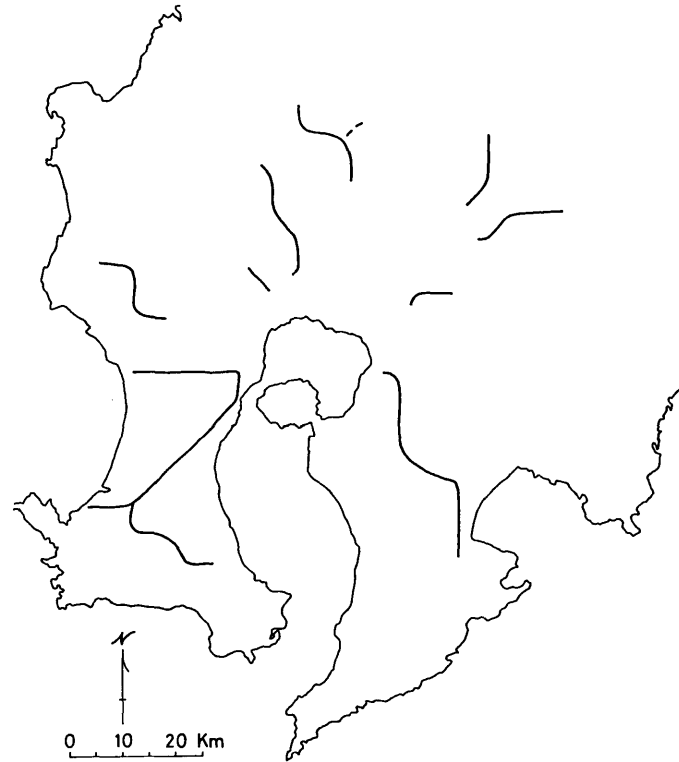Fig. 5.1.e. Md "Contour lines", using the overlapping means.

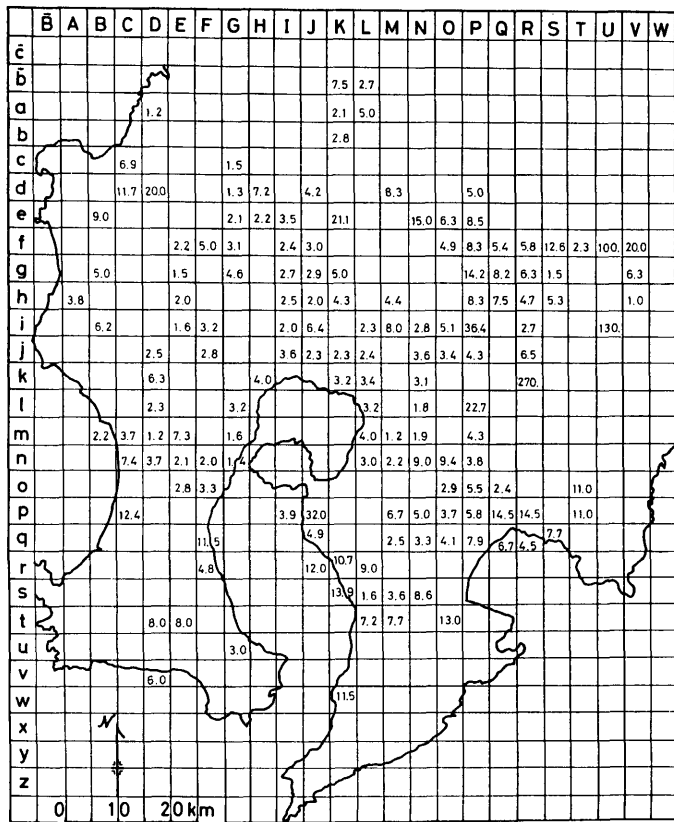Fig. 5.1.f. Md "Ride and valley lines", using the overlapping means.

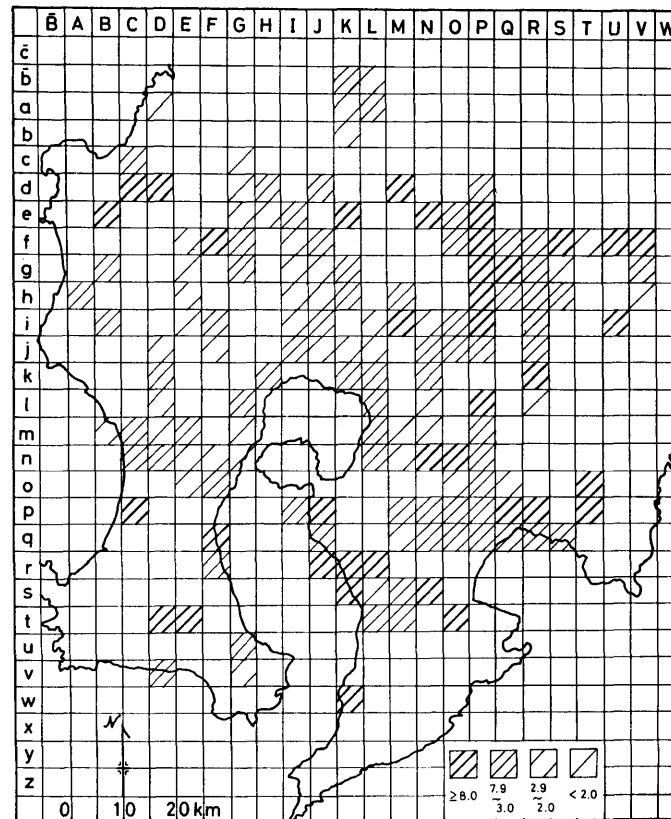Fig. 6.1.a. NPF/NLF "Data map". The arithmetic means of data calculated for every squares are plotted on a map.

	B̄	A	B	C	D	E	F	G	H	I	J	K	L	M	N	O	P	Q	R	S	T	U	V	W
c̄																								
b̄											7.5	2.7												
a					1.2						2.1	5.0												
b											2.8													
c				6.9				1.5																
d				11.7	20.0			1.3	7.2		4.2			8.3			5.0							
e		9.0					2.1	2.2	3.5		21.1				15.0	6.3	8.5							
f						2.2	5.0	3.1		2.4	3.0					4.9	8.3	5.4	5.8	12.6	2.3	100.	20.0	
g			5.0			1.5		4.6		2.7	2.9	5.0					14.2	8.2	6.3	1.5			6.3	
h		3.8				2.0				2.5	2.0	4.3		4.4			8.3	7.5	4.7	5.3			1.0	
i			6.2			1.6	3.2			2.0	6.4		2.3	8.0	2.8	5.1	36.4		2.7			130.		
j					2.5		2.8			3.6	2.3	2.3	2.4		3.6	3.4	4.3		6.5					
k					6.3				4.0	3.2	3.4		3.1						270.					
l					2.3		3.2				3.2		1.8		22.7									
m		2.2	3.7	1.2	7.3		1.6			4.0	1.2	1.9		4.3										
n			7.4	3.7	2.1	2.0	1.4			3.0	2.2	9.0	9.4	3.8										
o					2.8	3.3									2.9	5.5	2.4			11.0				
p				12.4				3.9	320			6.7	5.0	3.7	5.8	14.5	14.5			11.0				
q						11.5		4.9				2.5	3.3	4.1	7.9			6.7	4.5	7.7				
r							4.8		12.0	10.7	9.0													
s									13.9		1.6	3.6	8.6											
t					8.0	8.0					7.2	7.7		13.0										
u							3.0																	
v					6.0																			
w										11.5														

0 10 20 km

Fig. 6.1.b. NPF/NLF "Hatching diagram".

≥8.0 7.9/3.0 2.9/2.0 <2.0

0 10 20 km

Fig. 6.1.c. NPF/NLF "Hatching diagram", using the over-
lapping $\frac{1}{4}$ means.

Fig. 6.1.d. NPF/NLF "Contour lines".

Fig. 6.1.e. NPF/NLF "Contour lines", using the overlapping means.

Fig. 6.1.f. NPF/NLF "Ridge and valley lines", using the overlapping means.

Fig. 6.2.a. NPC/NLC "Data map". The arithmetic means of data calculated for every squares are plotted on a map.
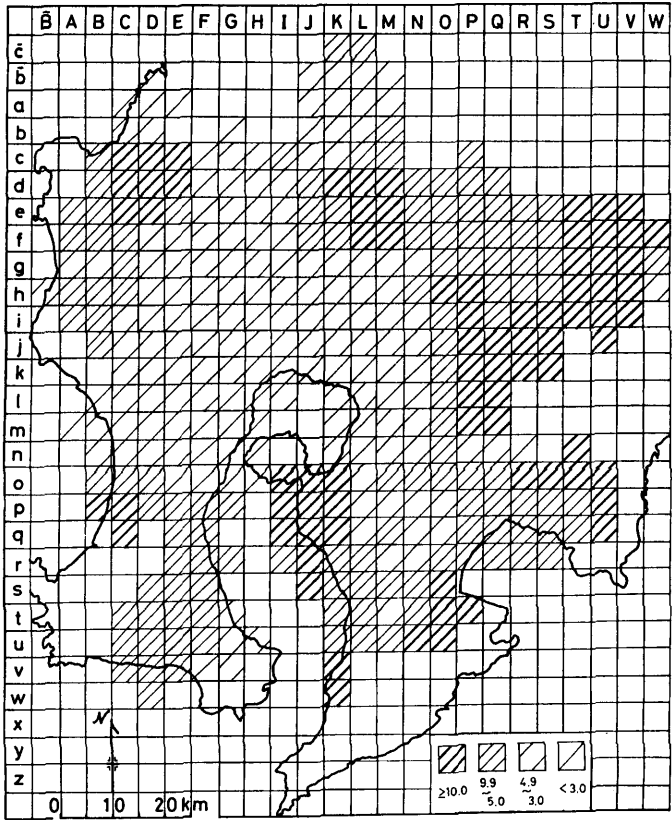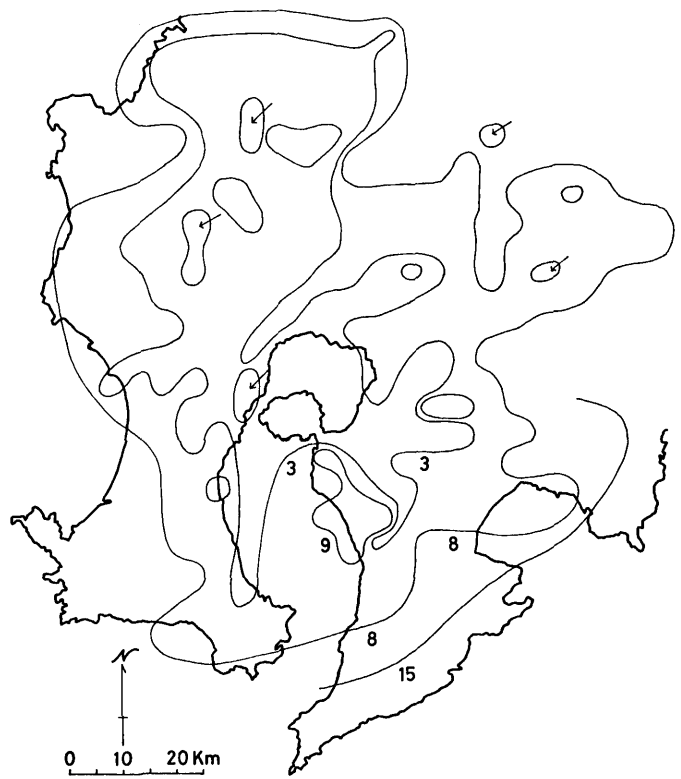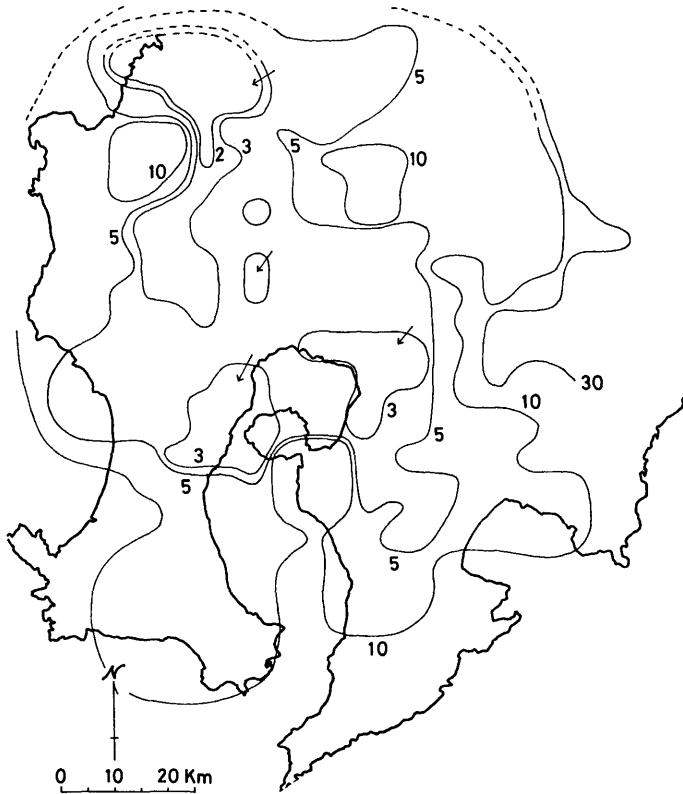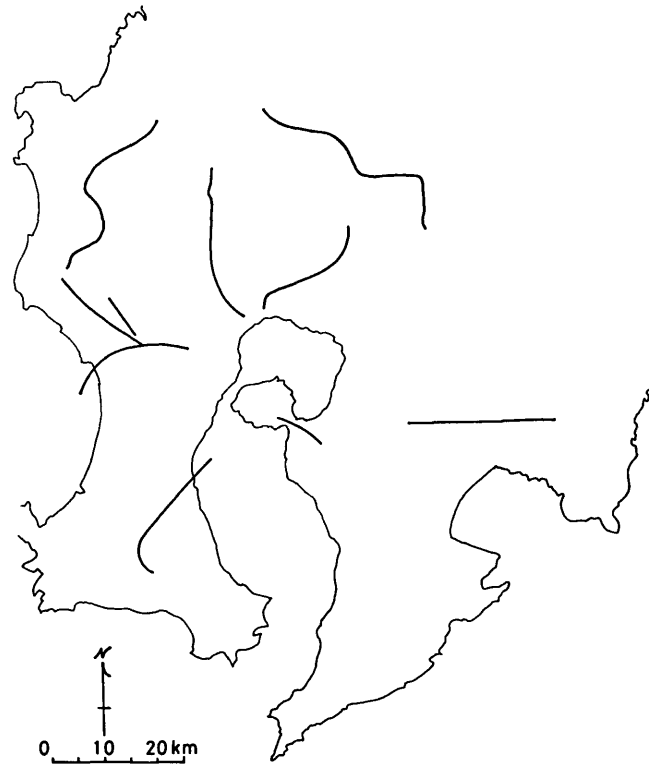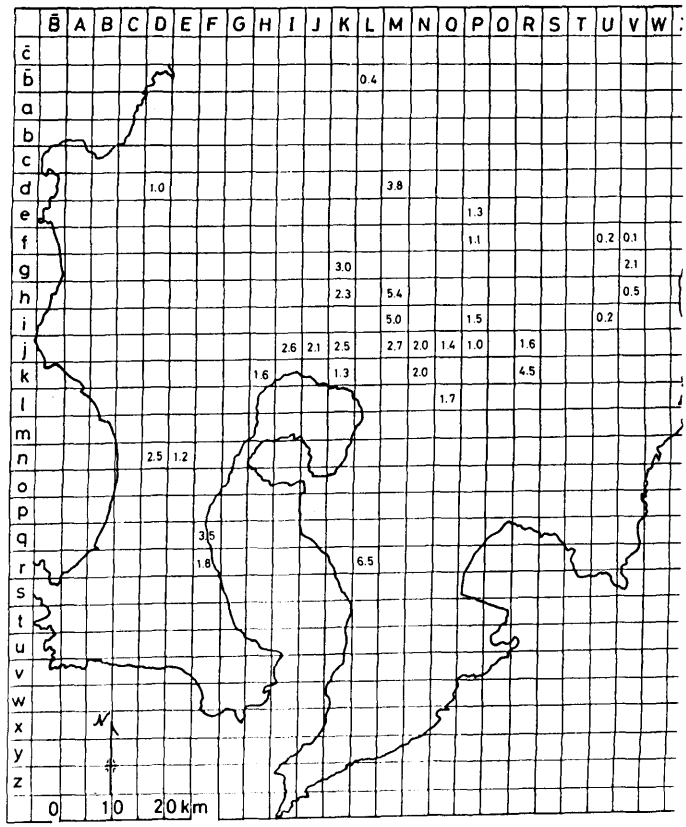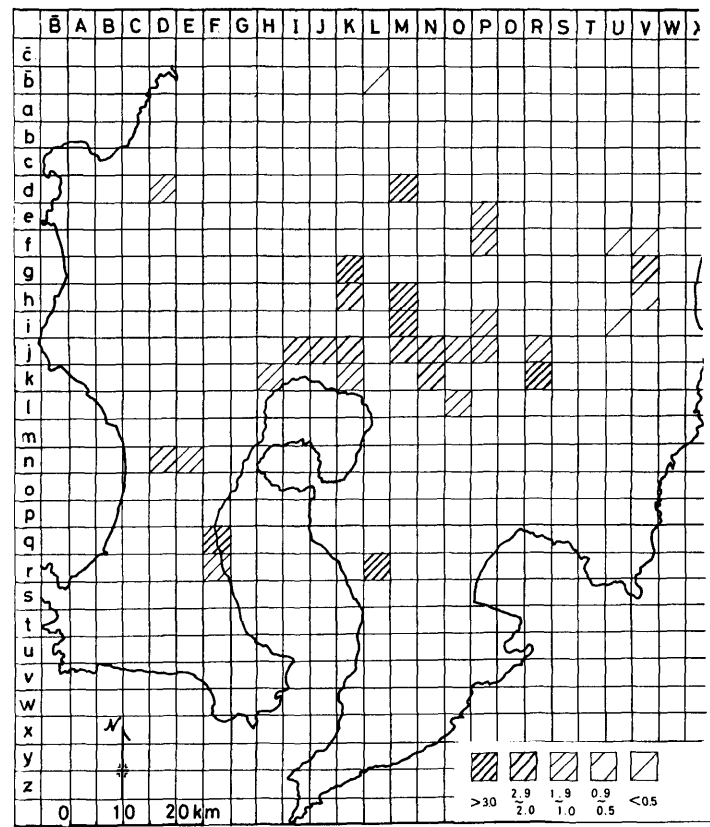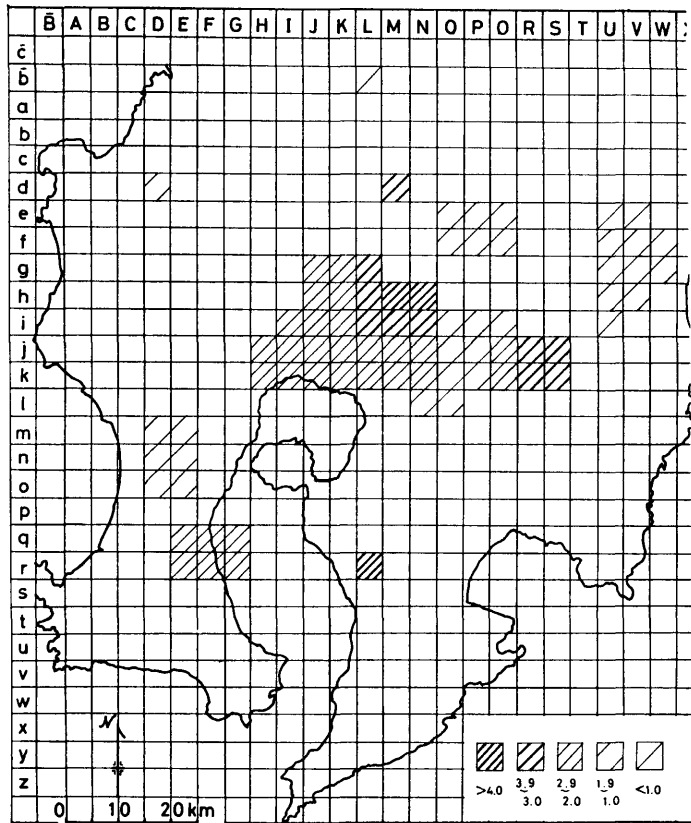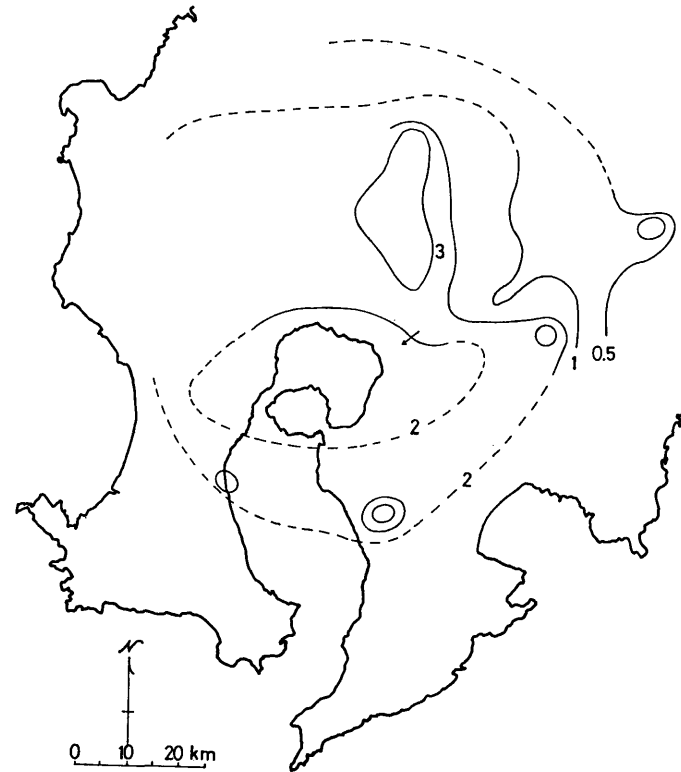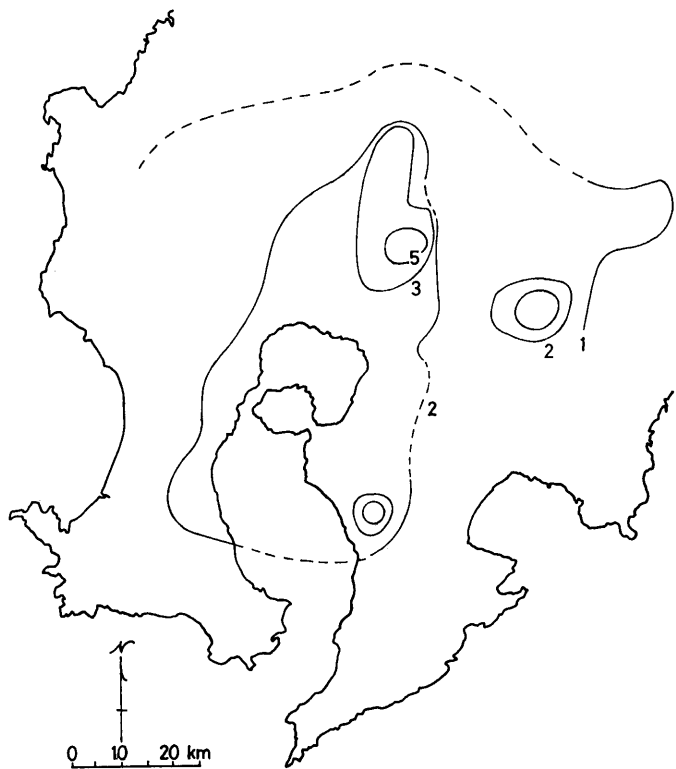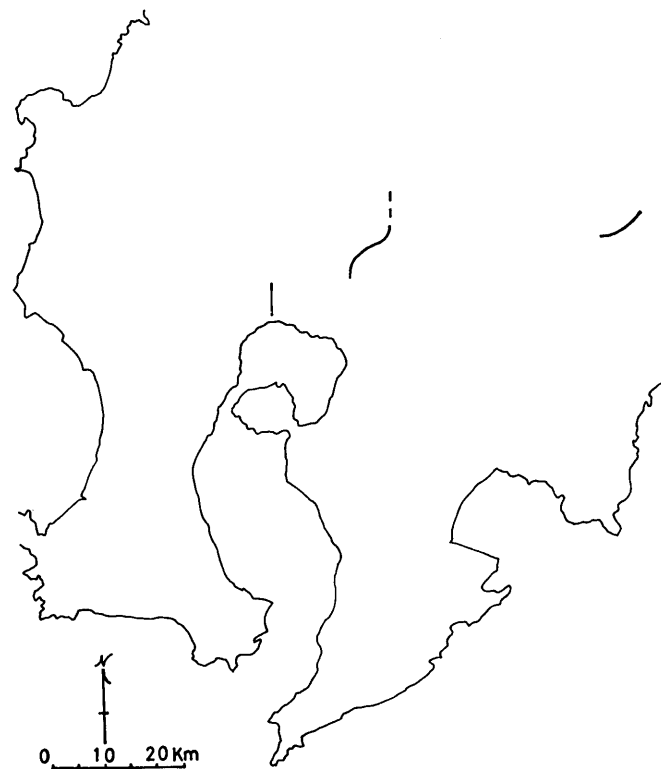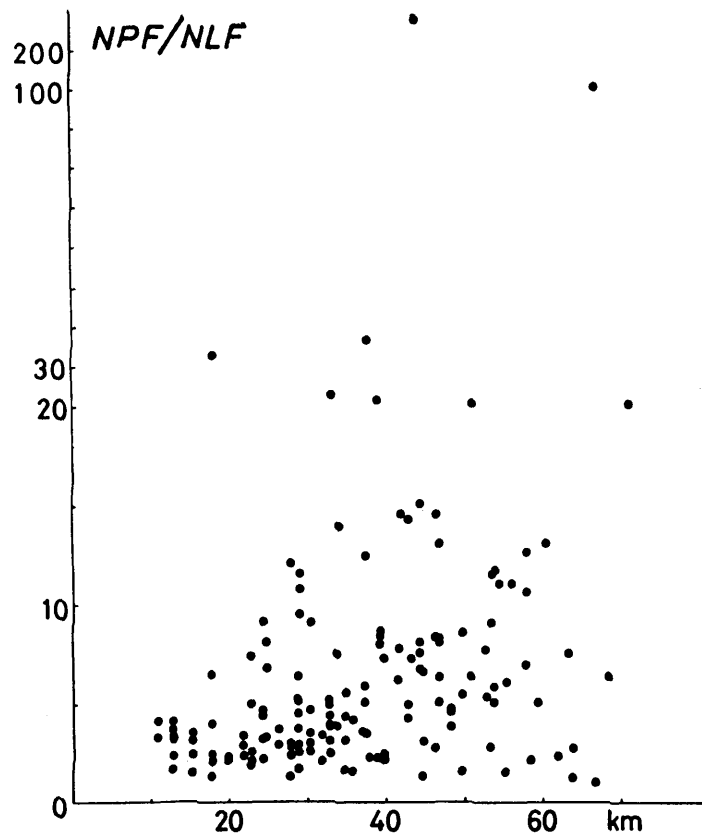

Fig. 6.2.b. NPC/NLC "Hatching diagram".

Fig. 6.2.c. NPC/NLC "Hatching diagram", using overlapping means.

Fig. 6.2.d. NPC/NLC "Contour lines".

Fig. 6.2.e. NPC/NLC "Contour lines", using the overlapp-
ing means.

Fig. 6.2.f. NPC/NLC "Ridge and valley lines", using the
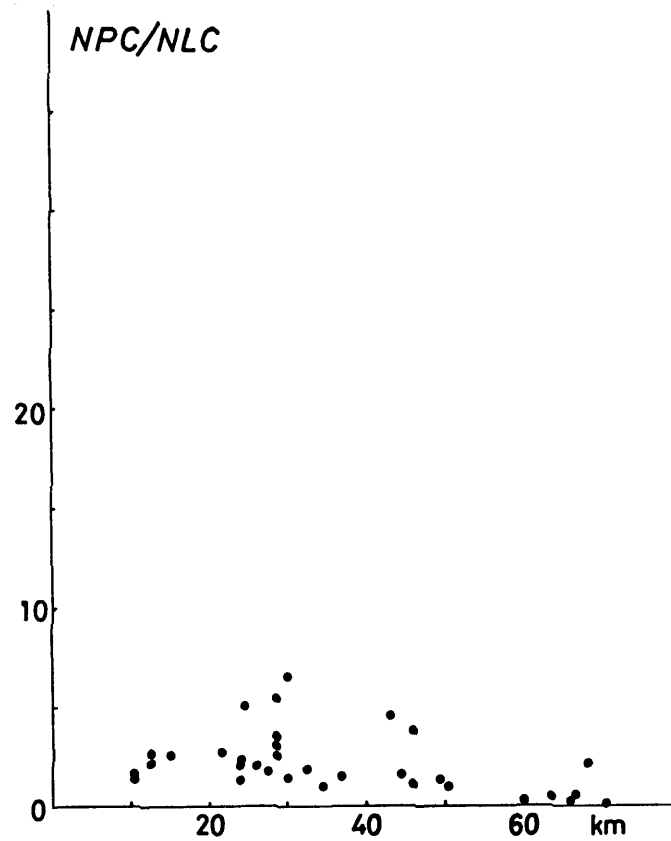overlapping means.

Fig. 6.3.a. Plot of NPF/NLF vs. D (km.)
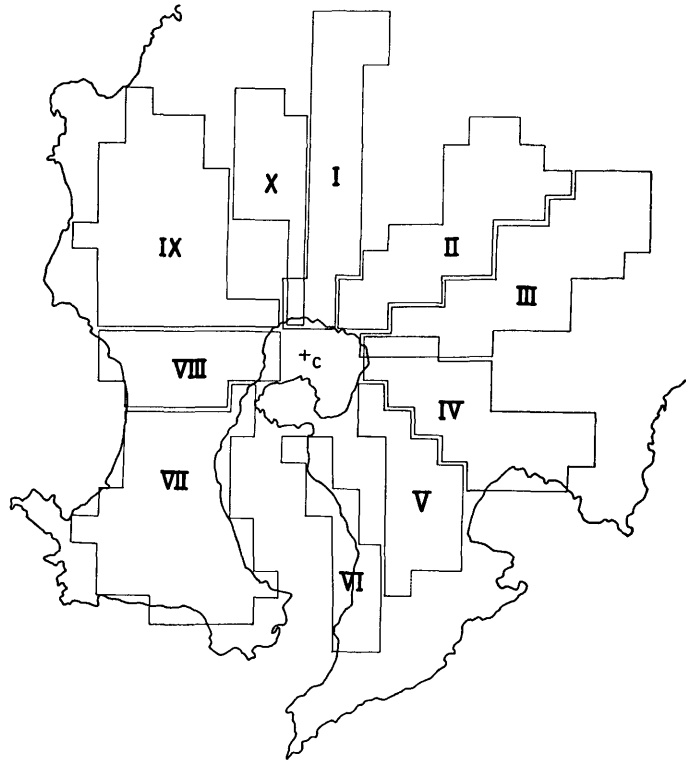

Fig. 6.3.b. Plot of NPC/NLC vs. D (km.)

Fig. 7.1. Showing the radial division of the localities where the measurements were carried out.
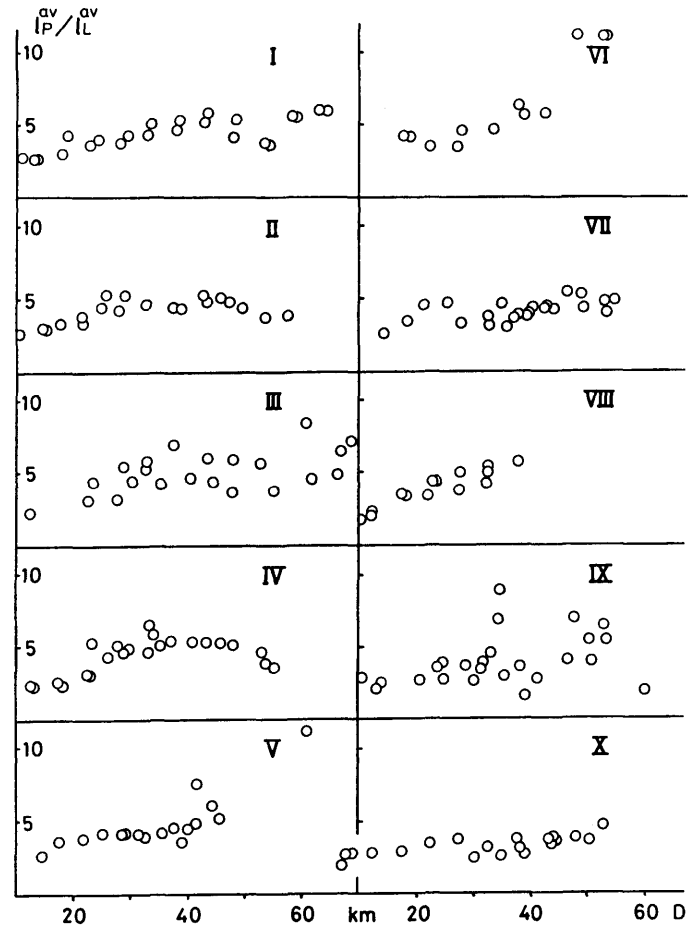C: Center of the Aira Caldera.

Fig. 7.3. Showing the relation between l_P^{av}/l_L^{av} and D (km).